Heliyon 10 (2024) e26493

Contents lists available at ScienceDirect

Heliyon

journal homepage: www.cell.com/heliyon

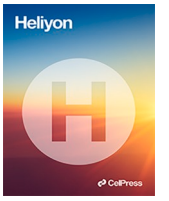

Research article

Thermal and hydraulic performance of ZnO/EG based nanofluids in mini tubes of different diameters: An experimental investigation

Muhammad Ahsan [a], Adnan Qamar [a], Rabia Shaukat [a], Habib-ur-Rehman Siddiqi [a], Zahid Anwar [a], Muhammad Farooq [a], Muhammad Amjad [a], Shahid Imran [a], Mansoor Ahmed [b], M.A. Mujtaba [a], H. Fayaz [c,*], Basma Souayeh [d,e]

[a] *Department of Mechanical, Mechatronics and Manufacturing Engineering, University of Engineering and Technology Lahore, New-Campus, Pakistan*
[b] *ZI Engineering, PC 10 Fifth Street, Third Floor Suite 303, Valley Stream, NY, 44581, United States*
[c] *Modeling Evolutionary Algorithms Simulation and Artificial Intelligence, Faculty of Electrical and Electronics Engineering, Ton Duc Thang University, Ho Chi Minh City, Viet Nam*
[d] *Department of Physics, College of Science, King Faisal University, P.O. Box 400, Al-Ahsa, 31982, Saudi Arabia*
[e] *Laboratory of Fluid Mechanics, Physics Department, Faculty of Sciences of Tunis, University of Tunis El Manar, Tunis, 2092, Tunisia*

A R T I C L E I N F O

Keywords:
Compact channels
Ethylene glycol
Frictional losses
Heat transfer coefficient
Nanofluid
Nanoparticle
Stability
Thermal conductivity
Viscosity

A B S T R A C T

The present experimental study investigates the thermal and hydraulic performance of Ethylene Glycol (EG)-based ZnO nanofluids (NFs) in circular minichannel test sections, each of 330 mm in length and 1.0–2.0 mm inner diameters. The experiments were conducted under steady-state constant heat flux and laminar flow conditions. The stable ZnO/EG-based NFs were synthesized using a standard two-step method in varying nanoparticles (NPs) loadings (0.012–0.048 wt %). The morphological characteristics, crystal structure, and specific surface area (SSA) showed that the NPs were sized in nm, possessing excellent crystal structure and enhanced surface area. Thermal conductivity (TC) and viscosity (VC) of the NFs were examined in the 20–60 °C temperature range. Both TC and VC possessed an increasing trend with the rise in concentration of the NPs. However, with the temperature rise, TC increased while the VC decreased and vice versa. The highest enhancements in TC and VC were 14.38 % and 15.22 %, respectively, at 40 °C and 0.048 wt% of NPs loading. The highest enrichment recorded in the local and average heat transfer coefficient (HTC) were 14.80 % and 13.48% in a minichannel with 1.0 mm inner diameter, respectively. It was directly proportional to the NPs loading and volume flow rate of the NFs. The friction factor was also directly proportional to the test section's inner cross-sectional area, while the pressure gradient showed an inverse behavior. An inverse relationship was recorded for the volume flow rate of the NFs and vice versa. Maximum friction factor and the pressure drop for all three minichannel test sections were recorded as 34.58 % and 32.16 %, respectively. The well-known Shah correlation predicted the local and average HTC within ±15.0 %, while the friction factor and the pressure gradient were well predicted by the Darcy correlation within the ±10.0 % range.

* Corresponding author.
E-mail address: fayaz@tdtu.edu.vn (H. Fayaz).

https://doi.org/10.1016/j.heliyon.2024.e26493
Received 5 October 2023; Received in revised form 14 February 2024; Accepted 14 February 2024
Available online 19 February 2024

1. Introduction

High heat flux management is the need of the hour in many industrial and commercial thermal applications. The cooling of compact-sized next-generation modern devices and systems is a significant concern for thermal engineers for their high performance and increased operational life [1]. Due to conventional fluids' limited heat transfer capability, researchers have been working for decades to use alternative fluids with better heat transfer and flow properties to manage high heat flux from such systems. The search ended with the invention of novel fluids, famously known as nanofluids (NFs). These newly invented NFs replaced conventional heat-exchanging fluids with better thermal performance [2]. The potential of these NFs has been investigated for effectively managing high heat flux from the aforementioned systems. In addition, scientists have been trying for decades to overcome the governing issues encountered for the commercial applications of NFs in different heat transfer systems [3].

Nanofluids (NFs) are a combination of nanometer-sized metallic and metal-oxide nanoparticles (NPs) suspended in the host base fluids (BFs). The heat-carrying capability of the NFs primarily depends upon the thermal characteristics of dispersed NPs. This is the key characteristic to overcome the high heat flux from modern high-tech devices [4]. Multiple efforts have been made in this regard by dispersing discrete types of metallic and meta-oxide NPs in the host BFs, like deionized water (DIW), distilled water (DW), and EG Ref. [5]. Recently, researchers have shown interest in dealing with metal oxide NFs due to their growing potential applications in different thermal systems [6]. Another reason for considering metal oxide-based NPs for synthesizing the NFs is their low density compared to the parent metals, leading to better dispersion stability in the host BFs. In addition, micro and minichannel heat-exchanging systems have also been explored using conventional cooling agents. However, integrating the NFs with the aforementioned heat exchanging system could exponentially enhance the HTC with a minimum quantity of NFs and more surface area available for heat transfer [7]. Al_2O_3, CuO, TiO_2, and SiO_2 are the most investigated NFs in different types of BFs in conventional and compact channels. However, less attention has been paid to the ZnO/EG-based NFs. The possible reasons can be a slightly higher true and bulk density of the ZnO NPs than most of the other metal oxide NPs and a comparable thermal conductivity not higher than the other NPs from this family. However, despite the facts elaborated, the ZnO/EG-based NFs can be used for heat transfer enhancement with reasonably good effectiveness, primarily when operating in low-temperature zones below the freezing temperature of the water [8].

In a research study, Kaggwa et al. [9] examined CuO/EG-based NFs for their dispersion stability using arabinogalactan (ARB) as a stabilizing agent. They found the stability of NFs for up to 20 days without any significant signs of sedimentation. The high stability recorded shows that the ARB's structural nature allows complete dispersion and solubility of CuO NPs within the host BFs. Jumpholkul et al. [10] examined SiO_2/DIW NFs (0.5–2.0 vol %) prepared using 2.0 h of ultrasonication for analyzing the stability. They found that the prepared NFs did not show any signs of sedimentation for the complete duration of the experimentation. In another study, He et al. [11] examined TiO_2/DW NF's stability for several months under an ultrasonication time of 30 min by analyzing the pH and zeta potential of NPs. All the studies conclude that the physical and chemical methods affect the NF's stability. The single techniques or a combination of both can be used to formulate the NFs as and when desired, dependent upon the nature of BFs and the NPs used.

The NF's temperature and the NPs concentration with the host BFs primarily influence the TC of the NFs. A similar observation was investigated for EG-based Al_2O_3 NFs by Gallego et al. [12] at 25 wt% of NPs. The maximum enhancement in the TC was 19.0 % compared to BFs. Kanti and Maiya [13] studied the TC enrichment of graphene oxide (GO) based NFs dispersed in DIW using polyvinylpyrrolidone (PVP) as a stabilizing agent. The minimum and maximum TC amplification in pure GO-based NFs was 36.8 % and 52.4 % at 30 and 60 °C, respectively, compared to DIW. It was also observed that the TC amplified as usual with the NPs loading and operating temperature. The highest TC recorded is also attributed to the possible reason for the relatively higher TC of GO NPs compared to other metal oxides. Karthikeyan et al. [14] found an enhancement of 31.6 % in the TC of CuO/H_2O NFs using a customized TC measurement system. They observed that NPs clustering harms the TC of NFs. Guo et al. [15] investigated the TC of SiO_2 (20 nm) with an optimized THW method at 20 °C. The TC of NFs under study was found to be 1.0–3.4 %, at 0.5–1.0 vol % loading of NPs. Sonawane et al. [16] examined the TC of TiO_2 NFs in an aqueous media. They found a maximum enhancement of 2.95 % and 22.131 % for 1.0 vol % and 6.0 vol % of NPs concentration at 25 °C. They used NPs of minimal size (4–8 nm); however, it seems a lesser NPs size could not contribute much towards the TC enhancement of NFs. Jeong et al. [17] inspected the NPs shape effect on the TC of ammonium polymethacrylate stabilized ZnO/DIW NFs using the THW method with an NPs size of 20–40 nm. They observed an increment of 16.0 % in TC at 5.0 vol % of NPs. Their study also confirmed that the spherical NPs possessed higher TC than non-spherical NPs due to their regular shape and specific surface area for heat transfer in the host BFs. Li et al. [18] investigated the TC of ZnO/EG-based NFs in 15–55 °C with mass concentrations of 1.75–10.50 wt %. A similar trend for TC enhancement was investigated as observed in the literature with temperature and concentration of NPs. Gallego et al. [19] examined the effect of operating temperature of NFs and the volume fraction of NPs on the TC of homogeneous and stable ZnO/EG NFs. The experimental results proved that TC increased nonlinearly with the NP's loading and operating temperature and vice versa. The non-liner behavior may attribute to the operating conditions, the NPs size and the specific surface area available for heat conduction between the NPs and the host BFs.

Kole et al. [20] experimentally investigated ZnO NPs dispersed in EG for their TC in a 10–70 °C temperature range for NPs loading of 0.5–3.75 vol % under an extensive ultrasonication of 60 h. The maximum rise in TC was recorded as 40 % (3.75 vol % of NPs) compared to the host BFs at a temperature of 30 °C. The TC of NFs was directly proportional to the sonication time and attained its maximum value at 60 h of sonication. This is probably due to enhanced stability and uniform distribution of the NPs within the host BFs. Moosavi et al. [21] investigated the TC of ammonium citrate stabilized ZnO/EG-based NFs in a 10–50 °C temperature range and observed a direct non-linear behavior of the TC with the temperature and concentration of NPs. A maximum 10.5 % rise in TC was recorded at 3.0 vol % of the NPs. Yu et al. [22] examined a similar kind of behavior, where they found an enhancement of 26.5 % in the TC of ZnO/EG-based NFs for 5.0 vol % of NPs in the 10–60 °C temperature range. The research findings for the TC of numerous metal

oxide-based NFs in DIW and EG-based NFs showed the strong dependence of the TC on the NPs loading in the host BFs and the temperature changes under the steady state operating conditions. The NP's shape and size are also the influencing parameters; however, the literature surge shows that their impact is insignificant and less researched than the concentration of NPs and operating temperature. A possible reason is their governing effect compared to the other influencing parameters.

The influence of temperature and NPs loading on the VC of EG-based Al_2O_3 NFs was studied by Gallego et al. [12] in their study. At 25 wt % of NPs, they observed an enhancement of 19.0 % in VC compared to BFs. Priya et al. [23] investigated Tiron-stabilized non-spherical CuO NPs dispersed in DIW at 28–55 °C. An enhancement of 8.0 % in the VC was recorded for 0.016 vol % of NPs at 50 °C. Kaggwa et al. [9] used ARB as a stabilizing agent to prepare stable CuO/EG NFs and found an enhancement of about 17.0 % in the relative VC of NFs. Duangthongsuk and S. Wongwises [24] found a rise of 13.0 % in the VC of aqueous TiO_2 NFs at 0.2–2.0 vol % loading of NPs in the 15–35 °C temperature range. Similar findings were reported in another study [25] as a function of NPs loading and the NFs temperature. Li et al. [17] examined the NPs shape effect on the VC of ammonium polymethacrylate stabilized aqueous ZnO NFs in 0.05–5.0 vol % at an operating temperature of 25 °C. They found that the VC increased to 59.0 % at 5.0 vol % of NPs. The highest augmentation in VC, in this case, is most possibly due to the increased NPs loading, and the effect of NPs shape seems to be insignificant, as many litureture studies support that the spherical shape NPs have a low impact on the VC compared to non-spherical NPs. Yu et al. [22] examined the VC of ZnO/EG-based NFs in the 10–60 °C temperature range. They found that the NFs possessed a Newtonian behaviour at low concentrations of NPs. They observed that the NFs showed a shear thinning behaviour for the increased NPs loadings. This is possibly due to the increased aggregation rate of NPs for NPs loadings.

Li et al. [18] investigated the VC of ZnO/EG-based NFs in 15–55 °C with mass concentrations of 1.75–10.5 wt %. The NFs showed a similar trend with the change in concentration of NPs and the operating temperatures, as observed in the aforementioned findings for the other metal oxide-based NFs. The NFs also demonstrated Newtonian behaviour under the mass concentration of NPs less than 10.5 %. In another investigation, Gallego et al. [19] studied the effect of operating temperature and NPs loading on the VC of ZnO/EG-based NFs. The VC, as usual, possessed a linear increasing behaviour with the weight fraction of the NPs and an inverse proportion with the temperature. Yu et al. [22] analyzed a similar behavior, finding an enhancement in the VC of ZnO/EG-based NFs in the 10-60 °C temperature range. In their investigation, Kanti and Maiya [13] observed that the VC of GO/DIW-based NFs possessed a non-linear behavior with an increasing shear rate in a mass concentration of 0.1–1.0 vol % at a temperature ranging between 30 and 60 °C. The maximum enhancement in the VC was 177 % compared to DIW at 30 °C. In another study [26], the authors investigated the VC of Al_2O_3 and Fe_2O_3-based hybrid NFs in a mixture of DIW and EG. Their investigation revealed that as long as VC is dependent on the concentration of the NPs and operating temperature, the ratio of two different NPs in the host BFs also greatly affects the VC of the resulting NFs. The research findings comprising various oxide-based NPs dispersed in DIW and EG-based NFs showed the strong dependence of the VC on the NPs loading in the host BFs and the NF's temperature. The effect of the NPs size and shape is also important; however, less attention is given to this side in the existing literature for most of the investigated metal oxide-based NFs, possibly due to the governing effects of NPs concentration and operating temperatures.

The HTC of Al_2O_3/DIW-based NFs in a circular cross-section test section was investigated by Anoop et al. [27] within laminar flow conditions under constant heat flux. Two different sizes of NPs were used in the investigation, and the NFs tested with 45 nm-sized NPs showed a maximum rise of 25.0 % compared to 150 nm-sized NPs, around 11.0 %. Rea et al. [28] investigated laminar HTC of Al_2O_3/DIW NFs in a vertically heated tube (OD = 6.4 mm, ID = 4.5 mm, length = 1001) and found an increase of 27% at 6.0 vol % loading of NPs. Goudarzi et al. [29] studied the HTC of the Al_2O_3/EG-based NFs using different NPs loadings. The investigation was conducted on a car's radiator with different configurations and geometries. The investigation revealed an enhancement in the system's thermal performance by up to 9.0 % compared to pure BFs. Abdollahi et al. [30] studied the thermal-hydraulic behavior of CuO/DIW NFs in a microchannel heat sink using NPs of different diameters at varying concentrations. Under laminar flow conditions (Re = 1300), the results specify that increasing the NP's loading and decreasing the NP's size augmented the Nusselt number. At the same time, the hydraulic characteristics of the NFs did not affect significantly. Gupta et al. [31] examined the HTC of TiO_2/DW NFs inside a copper tube (ID = 8.0 nm, OD = 10 mm, L = 1.05 m) under laminar flow conditions. HTC of NFs was directly proportional to the NP's mass loading and fluid flow rates. An increment of 50.11 % was observed for 0.1–0.3 wt% of NPs, keeping other parameters constant. However, an inverse relationship between the HTC and NPs loading has been observed for 0.3–0.5 wt% of NPs. A possible reason may be the NPs clustering over time. Hashemi et al. [32] followed a similar trend for SiO_2/DIW NFs in a rectangular heat sink within a laminar flow regime. The maximum enrichment in the HTC was 3.5–5.0 % for the volume concentrations of NPs 4.0–8.0 %.

Ali et al. [33] examined the heat HTC of aqueous SHMP-stabilized ZnO NFs in a car radiator in various volumetric loadings. NFs showed an enhancement in the HTC than the host BFs for all the tested concentrations of NPs. A maximum 46.0 % enhancement in the HTC was recorded at NPs volume concentration of 0.2 %. Topuz et al. [34] observed an enhancement in the thermal performance of ZnO/DIW NFs of up to 1.5% compared to host BFs at 1.0 vol %. The HTC of aqueous ZnO/EG NFs were experimentally tested by Wen et al. [35] in two multiport tubes. Results showed that HTC growth was 6.7–9.8% for NPs concentrations of 0.75–1.50 vol %, at the expense of higher frictional losses of 4.6–8.6 %. ZnO/EG NFs were tested for forced HTC in spiral shell-tube heat exchangers at varied concentrations of ZnO nanorods (0.1–0.3 vol%) under laminar flow conditions at varying Reynolds numbers (400–600). The results show that adding minor concentrations of ZnO nanorods can dramatically improve the HTC [36]. A square-type heat sink thermal efficiency using/EG-based NFs at various ZnO NPs concentrations was examined in another study [37], at 0.10 wt % ZnO NPs, a 51.5 % increase in *Nu* number was observed. Furthermore, the average HTC increased to 1292 W/m^2K for ZnO/EG-based NFs. Kanti et al. [38] investigated that the HTC and thermal performance of the NFs greatly depend upon the NPs loading. However, as long as the HTC increases with the rise in the NP's loading, there is a significant drop in pressure and enhancement in the friction factor across the heat-exchanging system. In another study [39], the authors investigated the thermo-hydraulic performance of water-based fly-ash and flyash-Cu-based hybrid NFs. The findings revealed that compared to water and fly ash-based NFs, the HTC was higher for the hybrid

NFs. Marulasiddeshi et al. [40] examined the thermal performance of Al_2O_3 and Al_2O_3–CuO-based NFs in DIW under constant heat flux conditions at various Reynolds numbers and fluid inlet temperatures. The study showed that the HTC increased with fluid inlet temperature, velocity, and NPs concentration. They observed an enhancement in the HTC up to 121.5 % for hybrid NFs compared to pure Al_2O_3-based NFs. The literature surge targeting the thermal performance of different types of metal oxide-based NFs declared that the HTC of NFs is strongly influenced by the NPs loadings, the NFs volume flow rate, the heat exchanger geometry, type, and shape. All these parameters are indirectly linked in other ways with the Reynolds number of the NFs flowing and the surface area of the heat exchanging system.

The research work reported in the existing literature shows that the most investigated metal oxides are Al_2O_3, CuO, SiO_2, and TiO_2 in an aqueous media and EG as a BFs. However, the investigations on the thermophysical properties (TC and VC), HTC, pressure drop, and frictional losses of ZnO/EG-based NFs in compact circular minichannel heat exchangers are very limited. Hence, this research aims to investigate the aforementioned neglected performance parameters and indicators for ZnO/EG-based NFs in compact circular minichannels of variable inner diameters (1.0–2.0 mm) at ultra-low NPs loadings (0.012–0.048 wt %). The heart of the investigation is the impact of NPs loading, thermophysical properties (TC and VC) of NFs, the fluid flow rate and minichannels diameter on the HTC, pressure drop characteristics, and frictional losses of NFs across the compact channel test sections. The present work's potential applications include but are not limited to advanced electronics cooling, heat exchangers used in power plants and process industry, solar thermal systems, biomedical applications, high-power laser diodes, and space cooling.

2. Materials and methods

2.1. NPs and chemicals

ZnO NPs and the EG of analytical scale were imported from renowned US-based Companies named Nanostructured and Amorphous Materials, Inc. and Merck. The NP's average size, as provided by the manufacturer's datasheet, was 20 nm. The purpose of importing such small-sized NPs is due to their proven high heat transfer capability, as presented in the existing literature. The other governing physiochemical characteristics of the ZnO NPs, comprising of true density (ρ_{np}), TC, and specific heat capacity (C_p), were 5600 (kg/m^3), 29.0 (W/m.K), and 514 (J/kg.K), respectively, under standard atmospheric conditions.

2.2. Preparation of NFs

The present study synthesized ZnO/EG-based NFs following the standard two-step methodology, widely adopted for preparing metal oxide-based NFs as reported in the literature [41]. First, the NFs samples were prepared in mass concentrations varying from 0.012 to 0.024 wt% without using any stabilizing agent. The measured quantity of NPs using an analytical balance (AWU-220D Shimadzu) was added to EG under 1.0 h of stirring using a magnetic stirrer (Heidolph MR Hei-End) at 1000 rpms, followed by 3.0 h of bath ultrasonication (Elma E100H). The temperature of the NFs during preparation was precisely controlled in a thermal bath (TC-550MX) to avoid any adverse temperature effects.

3. Experimental setup and procedures

This section comprehensively describes the different analytical tools and techniques to study the thermophysical properties (TC and VC), thermal (HTC), and hydraulic characteristics of ZnO/EG-based NFs under the desired operating conditions. In addition, details about the procedures adopted to execute the experimental investigations and the limitations of each instrument are also well-elaborated. Finally, the critical specifications, uncertainties, and accuracies of the instruments used under the experimental operating conditions have also been well elaborated at the appropriate places.

3.1. Dispersion stability of ZnO/EG NFs

The uniform and homogeneous dispersal of NPs within the desired host BFs is essential for their practical use in thermal applications. Researchers have used different techniques to evaluate the NF's stability. These include but are not limited to the physical and chemical methods [42]. The current experimental study used the visual photography method for the subject purpose. Many researchers in existing literature used the subject method. First, the sedimentation rate of NPs was estimated by capturing snapshots of the glass vials containing NFs samples over an equal time for the complete duration of the investigation. All the snapshots were taken with great care and precision to avoid human errors. Then, the captured snapshots over the investigated time intervals were matched and contrasted to evaluate the stability of the ZnO/EG NFs over the studied period. The investigation was conducted in an isolated, vibration-free room with controlled environmental conditions. The method is friendly in the ease of its use and was used by many researchers in the existing literature [43].

3.2. Thermal conductivity of ZnO/EG NFs

The TC of the ZnO/EG-based NFs was measured using a precise and accurate thermal conductivity analyzer (TEMPOS-METER Group, USA). This method uses the famous THW method to evaluate the TC of NFs [44]. The investigation was carried out in the 20 to 60 °C temperature range for the mass concentrations of NPs ranging from 0.012 to 0.048 wt %. KS-3 needle sensor (TC range, 0.2–2.0

W/mK), simultaneously acting as a heating source and sensor to record the TC, was set in the standard glass vial containing the NFs samples. Before performing the experiments with the NFs samples, the subject sensor was calibrated using a standard solution of known TC, and the experimental uncertainty was estimated to be ±1.0 %. The testing was conducted acoustically and vibration-free to avoid convection errors. Since the TC of the NFs is sensitive to temperature fluctuations, any variation in the operating temperature directly influences the TC of the NFs. Hence, to ensure data accuracy, reproducibility, and repeatability, the system's temperature was maintained during the experimentation using a temperature-controlled bath to attain the desired temperature of the NFs.

3.3. Viscosity of ZnO/EG NFs

The ZnO/EG-based NF's VC was measured using a precise Rotary Rheometer (RHEOTEST RN 5.1). The investigation was carried out in the 20 to 60 °C temperature range for the mass concentrations of NPs ranging from 0.012 to 0.048 wt % in a shear rate ranging from 0.01 to 1000 s^{-1}. The instrument was calibrated using a standard fluid of known VC, and the instrument's uncertainty was within ±1.0 % of measured experimental findings. The system contains a built-in system for controlling and attaining the desired temperature of the NFs samples. The test setup was validated using a standard solution, and the deviation between the findings was within ±1.0 %. The NFs sample of the required quantity was filled in the sample holder of the Rheometer. Then, the system was operated under the desired operating temperature and shear rate to measure the dynamic VC of the ZnO/EG NFs.

3.4. Heat transfer coefficient of ZnO/EG NFs

In the present research study, the thermal (HTC) and hydraulic analysis of ZnO/EG-based NFs was made using different inlet diameters (1.0–2.0 mm) mini channel tubes of the same fixed length. This study used all the mini tubes of uniform cross-sectional area, fixed length (330 mm), and wall thickness (0.5 mm). The flow rate through each diameter's mini tube test section was maintained using a syringe pump with dual syringes (KDS Legato-200). The pump used two syringes, each of 120 ml, while the experimental data was measured under varying flow conditions through the test section (12–24 ml/min). The test rig schematic for executing the desired data is shown in Figs. 1 and 2.

The thermal (HTC) and hydraulic properties of the ZnO/EG-based NFs were examined within the mini tube test sections subjected to the constant heat flux boundary conditions. The heat flux was applied to the stainless-steel mini tubes by applying a direct current across the inlet and outlet using a DC power supply (LW-3060-KD). To evaluate the surface temperature of the mini tubes, 10-K type thermocouples were installed at the surface of the outer wall of the test section using an electrically insulated and thermally highly conductive epoxy (OB-101-1/2). The inlet and outlet temperatures of the fluid at the entry and exit of the test sections were examined using two independently installed thermocouples, which directly measured the fluid temperature. Finally, the hydraulic characteristics of the NFs were measured by installing a differential pressure transducer (HC-692, 0–1 bar). All the thermal and hydraulic data acquisition was done using a Keysight 34970A data logger.

The test setup was installed in a room with controlled environmental conditions to mitigate any adverse effects of atmospheric variations on the performance of the different sensitive instruments used for the data collection and acquisition. The system was insulated using fiberglass insulation to avoid unaccounted heat losses from the heated test sections. The experimental results across the test sections were recorded under controlled steady-state operating conditions.

3.5. Data analysis for ZnO/EG NFs

Different mathematical correlations and models are critical for calculating important parameters to investigate the HTC and pressure drop of NFs while flowing through the compact channel test sections. The measured parameters using precise instrumentation, such as temperatures, flow rates, pressure drop, and other physiochemical properties of the NFs and NPs, are the input parameters for calculating heat transfer and friction factor-related parameters. The mathematical models and correlations for calculating

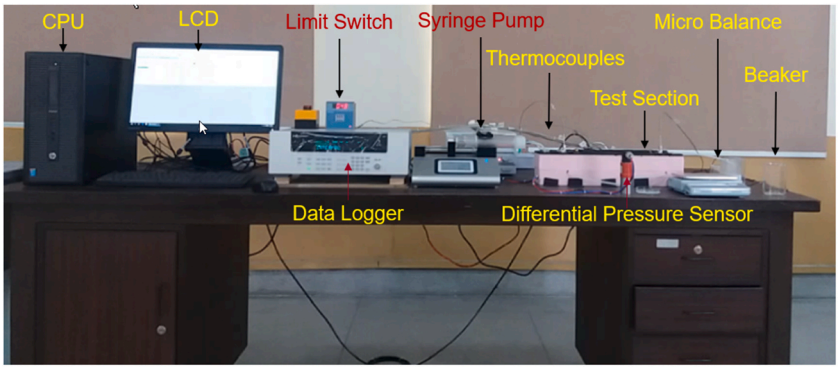

Fig. 1. Test rig setup for HTC and pressure gradient measurement of ZnO/EG NFs.

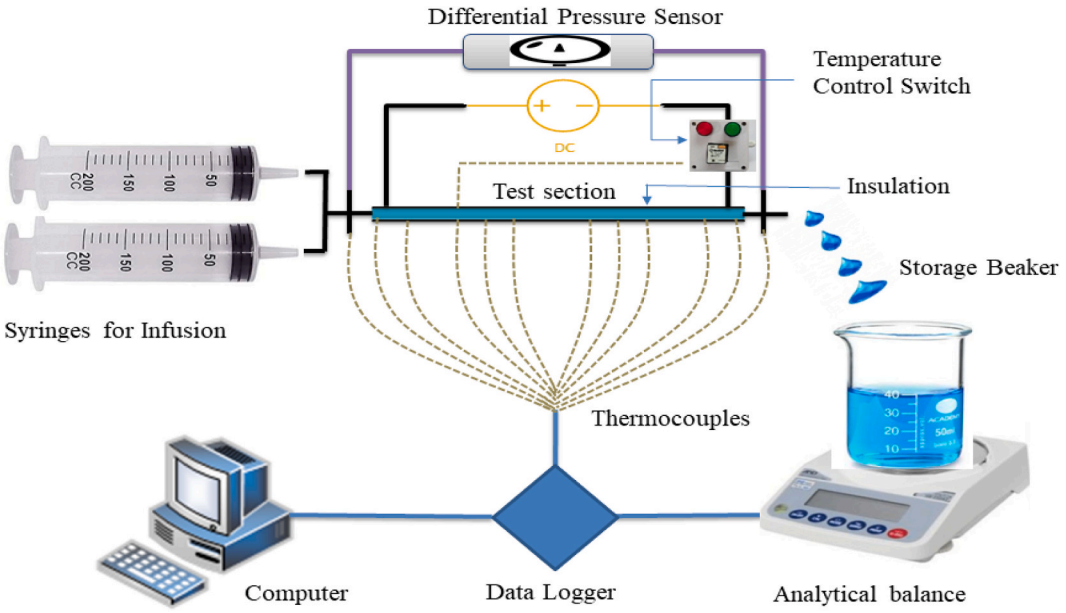

Fig. 2. Schematics of the test rig for HTC, pressure drop and frictional losses of ZnO/EG NFs in minichannels.

the subject properties and parameters of the NFs have been well elaborated in our previous study [45]. The theoretical modeling of the thermal and hydraulic performance of the NFs is carried out using the famous Shah's correlation and the Darcy correlation in laminar flow conditions. Mathematical expressions are also available in the subject study [45]. For the ease of graphical presentation of the experimental data sample, sample coding for the different concentrations of the ZnO/EG-based NFs has been clarified in Table 1. The same coding and symbols defined for the subject purpose have been used and presented in all of the text's graphical data representations.

3.6. Uncertainty analysis of ZnO/EG NFs

The significance of reported results lies in the precision of their repeatability in experimental outcomes. Various factors influence the uncertainty, each associated with the uncertainty in independent variables. For instance, if z is a variable and is a function of an independent parameter, Xi, each with its corresponding uncertainty (ΔXi), the overall uncertainty in z can be assessed using Eq. (1) [46].

$$\Delta z = \pm \sqrt{\sum_{i=1}^{n} \left(\frac{\partial f}{\partial Xi}\right)^2 (\Delta xi)^2} \tag{1}$$

In the present case, the uncertainty analysis performed for different independent and dependent variables is reflected in Table 2. This gives a brief insight into the percentage error and the error propagation within the measured and calculated thermal and hydraulic parameters studied in the research.

By acknowledging and accounting for these uncertainties, the experimental results presented in this study gain enhanced credibility and applicability, fostering a more robust foundation for subsequent analyses and interpretations.

4. Characterization of ZnO NPs

4.1. Scanning electron microscopy

In the present experimental study, the morphological properties of ZnO NPs were investigated using a Nova Nano 450 Scanning

Table 1
NFs sample coding for different concentrations of NPs and diameters of the minichannel test sections.

NPs + BFs (NPs loading)	Sample Coding	Tube Dimensions	Tubes Coding
ZnO + EG (0.012 wt %)	Z12E	Di + T = 1.0 mm + 0.5 mm	D1T
ZnO + EG (0.024 wt %)	Z24E	Di + T = 1.5 mm + 0.5 mm	D2T
ZnO + EG (0.036 wt %)	Z36E	Di + T = 2.0 mm + 0.5 mm	D3T
ZnO + EG (0.048 wt %)	Z48E	–	–

Table 2
Uncertainties of governing important independent and dependent parameters.

Governing Characteristics	Uncertainty	Governing Characteristics	Uncertainty
Diameter of Minochannels (D)	±0.001 m	Specific Surface Area of NPs (A_s)	1.09 %
Length of Minichannels (L)	±0.001 m	NFs Velocity in Minichannels (u)	2.76 %
Density of NFs (ρ)	±1.0 %	Reynolds Number of NFs (Re)	2.04 %
NFs Flow Rate ($\dot{m}$)	1.0 %	Friction Factor across Minichannles (f)	5.55 %
Specific Heat Capacity of NFs (c_p)	±1.0 %	Pumping Power Required (P)	2.07 %
Temperature Measurements (T)	±0.1 °C	Average HTC of NFs (h_{avg})	3.96 %
Thermal Conductivity of NFs (k)	±1.0 %	Average *Nu* of NFs (Nu_{avg})	4.54 %
Viscosity of NFs (μ)	±1.0 %	Local HTC of NFs (h_{local})	5.43 %
Pressure Gradient (ΔP)	1.25 %	Local *Nu* of NFs (Nu_{local})	5.67 %

Electron Microscopy (SEM). The SEM (Nova Nano 450) used in the present study possessed a high resolution and magnification of 1.0 mm and 500,000, respectively. Fig. 3(a) shows the NP's image at 100,000 magnifications. In addition, an analysis software (Image J) was used to investigate the size distribution of NPs, as shown in Fig. 3(b), and was found at about 33 nm. The NPs size was a little greater than the manufacturer-provided one, possibly due to the aggregation of NPs over time. Nevertheless, the findings are consistent with the manufacturer's specifications. A slightly larger size observed in the present case could be supposed to break down to the original ones during the preparation of the NFs.

4.2. X-ray diffractometry

The dry ZnO NPs samples were examined using an X-ray diffractometer (Burker D2-Phaser). The X-ray diffraction (XRD) pattern of the ZnO NPs is presented in Fig. 3(c). The XRD analysis showed unique line-broadening peaks, indicating that the ZnO NPs are nanostructured. The XRD patterns' peak intensity, location, and breadth were determined at fullwidth at half-maximum (FWHM) data. The hexagonal wurtzite phases of the subject ZnO NPs with lattice constants a = 3.24 A°, b = 3.24 A° and c = 5.21 A° showed the deflection peaks at 31.83°, 34.51°, 36.32°, 47.62°, 56.70°, 62.95°, 68.12°, and 69.17°. These indexed well match those in JCPDS card numbers 036–1451 [47]. Furthermore, it reflects the highest purity and excellent crystalline nature of the ZnO NPs. In addition to the SEM analysis, the NPs size was also estimated from the XRD graph using the Debye-Scherrer correlation presented in Eq. (2) [48]. This

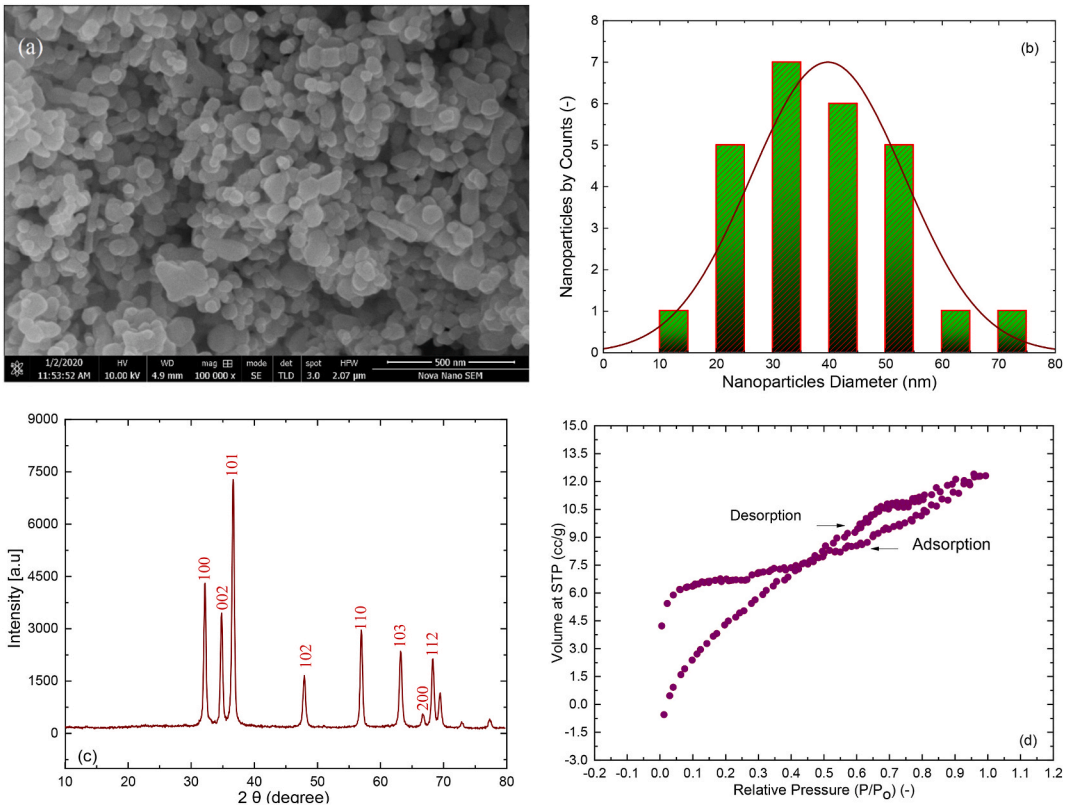

Fig. 3. ZnO NPs (a) SEM analysis (b) size distribution (c) XRD spectrum (d) BET analysis.

correlation gives a rough estimate of the crystal size of the NPs and is frequently used by many researchers in their studies to estimate the size of NPs.

$$D = \frac{K \times \lambda}{\beta \times \cos\theta} \tag{2}$$

here, "D" is the crystallite size of the particle, "K" is the shape factors and is a dimensionless number; typically, its value is around 0.9. "λ" is the wavelength of X-rays radiations, "β" is the FWHM of the diffraction peak and "θ" is the diffraction angle. In the present case, the average NPs size calculated using Eq. (1) was 18.46 nm. This slightly differs from the SEM investigation, possibly due to an uneven size distribution of NPs, as reflected in Fig. 3(b).

4.3. Brunner-emmet-teller analysis

The most widely used technique in the existing literature to evaluate the NP's specific surface area (SSA) is the Brunauer-Emmett-Teller (BET) method to determine its potential effect on the heat transfer properties of the formulated NFs. The adsorption/desorption characteristics of the nitrogen (N_2) gas are used to evaluate the SSA of the NPs. In addition, a volume flow methodology was used to measure the adsorbed quantity of the liquified nitrogen (N_2) gas [49]. This study used a highly precise and accurate SSA analyzer (NOVA 3200e) to evaluate the ZnO NPs SSA. After degassing the specimens (146 mg) at 100 °C for 5.0 h, the SSA of the NPs was measured using the BET analyzer based on the nitrogen (N_2) adsorption/desorption data of isotherms. This research estimated the mean pore diameter (size) and the volume of the ZnO NPs using a Barrett-Joyner-Halenda (BJH) technique. Fig. 3(d) depicts ZnO NPs' adsorption and desorption isotherms, and the SSA was approximately 22.37 m^2/g. Due to possible aggregation of the NPs over time the measured SSA was slightly different from the manufacturer-specified SSA. However, it is supposed to attain the original value during the NFs preparation. Fig. 3(d) illustrates valuable insight into the gas adsorption behavior on the surface of ZnO NPs. The information regarding the available SSA for the gas adsorption, the pore size distribution, and the adsorption capacity of the NPs can also be easily grabbed. The behavior of the adsorption-desorption isotherm, shown in Fig. 3(d), shows mesoporous structures within the ZnO NPs. The hysteresis loop also confirms that the adsorption process is not entirely reversible, and the shape of the hysteresis loop further confirms the rigid mesoporous structure of ZnO NPs with a broad pore size distribution.

5. Results and discussions

5.1. Stability of ZnO/EG NFs

The stability inspection results for the EG-based ZnO NFs for various concentrations of NFs have been shown in Fig. 4(a) and (b). The photographs captured just after the preparation presented in Fig. 4(a) show the uniform dispersion of the subject ZnO-based NPs within the under-consideration host BFs. The milky color of the formulated NFs also indicates that the NPs aggregates formed during the storage were dissociated to their original size, as mentioned by the manufacturer. The photographs captured after 24 h showed no signs of NPs sedimentation, as presented in Fig. 4(b). 40 ml special transparent glass vials (CNW, Singapur) have been used in this research study. The experimental findings showed no visual signs of NPs sedimentation over the investigated time, showing reasonable stability of the NFs. Furthermore, the prepared samples of the NFs were found stable for an observation period of 30 days. The investigation confirmed the stability of NFs for a long duration and its consistency with the literature for applying prepared NFs in mini-compact channels. The long-term stability of the NFs is attributed to the uniform dispersion of the NPs under acute sonication and stirring processes as adopted for the preparation of NFs in the present research. The ZnO NPs are supposed to possess the robust electrostatic force of repulsion within the host BFs, which prevents them from aggregation. As the existing literature supports, a reasonable charge on the NPs could result in stable NFs with excellent thermophysical properties [50].

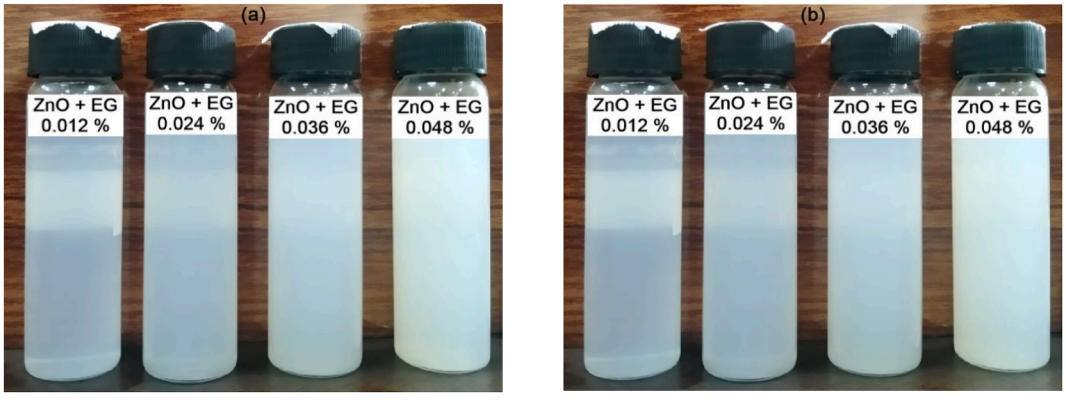

Fig. 4. ZnO/EG NFs (a) after preparation and (b) after 24 h.

The existing literature revealed very high-tech and expensive instrumentation for the stability investigation of the NFs; however, these instruments are not readily available to everyone due to their high cost and require expertise in operating and handling them [51]. However, the visual photography method can easily estimate the stability of the NFs forming colored dispersions without requiring the involvement of high-tech instrumentation and skills. The only pre-requisite is taking the snapshots carefully in a vibration-free environment.

5.2. Thermal conductivity of ZnO/EG NFs

TC of ZnO/EG-based NFs varies directly with the temperature and mass concentration of NPs, as presented in Fig. 5(a). At a temperature of 40 °C, the rise in TC of NFs compared to EG was 4.92–14.38 % for 0.012–0.048 wt %. The rise in temperature of the NFs triggers the NP's Brownian motion within the host BFs, which contributes towards enhancing the overall TC of the system. The interfacial layer between the host BFs and the NPs contributes to TC enrichment. The increase in NPs loading makes it more convenient for the enhancement in the TC of NFs due to the enrichment of more conducting materials within the host BFs. The highest recorded TC in the present case is also attributed to the smallest size and spherical shape of the NPs, hence the availability of more SSA of the NPs exposed in the host BFs environment [52]. Similar findings have been reported in a study [48] with ZrO_2/EG-based NFs at 0.2–1.0 vol % and 20–60 °C temperature range. The TC of the ZrO_2/EG-based NFs augmented with the NP's loading and operating temperature. The experimental results of the present study were compared with the aforementioned study at a temperature of 60 °C. It was found that the enhancement in TC was 5.11–14.55 % for the NPs mass concentration of 0.012–0.048 %, while for ZrO_2/EG-based NFs, this enhancement was 7.60–19.60 % in the volume concentration of 0.2–1.0 %. The higher TC reported in the case of ZrO_2/EG-based NFs is possibly due to the higher mass concnentration of ZrO_2 NPs in the host BFs. The other possible contributing parameters are the TC of the NPs, their morphology, nature, and dispersion stability in the BFs. It attributes to the fact that the TC of the NFs is not dependent only on the operating temperature of the system but also on the nature of the NPs, the concentration of the NPs in the host BFs, and the size and shape of the NPs.

The research results found in the present case for TC of NFs were compared and contrasted with a study [45] conducted by the authors using ZnO NPs in the DIW under similar concentrations of the NPs and operating temperatures, as presented in Fig. 5(b). The comparison showed that the operating temperature and the NPs loading influenced the TC of NFs in the same manner in both cases. An increasing trend was observed in the TC of the NFs, with a rise in the concentration of the NPs and the operating temperature of the NFs. However, EG-based NFs showed relatively lower TC than DIW-based NFs under the same operating condition. This is possibly due to EG's relatively lower TC than DIW's. This also revealed that the NFs' TC is not only linked with the characteristics of the NPs but also

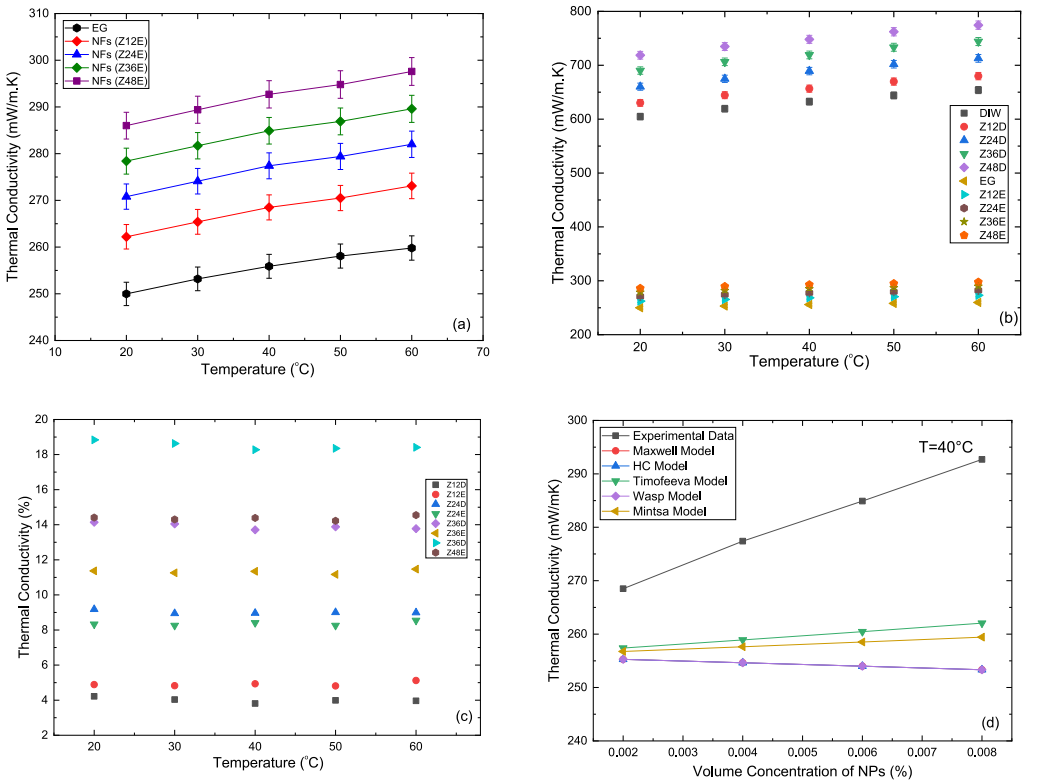

Fig. 5. ZnO/EG NFs TC (a) function of temperature and NPs loading (b) comparison with classical models.

highly dependent upon the properties of the host BFs. Z12D, Z24D, Z36D, and Z48D present the mass concentrations of 12 mg, 24 mg, 36 mg and 48 mg, respectively, in DIW.

Fig. 5(c) shows the percentage enhancement in the TC of the ZnO/EG-based NFs compared to the host BFs. It was recorded that the highest TC of the ZnO/EG-based NFs was at a temperature of 60 °C and a concentration of NPs of 0.048 wt % Fig. 5(d) compares the experimental findings for the ZnO/EG NFs with those estimated from the classical correlations. The investigation showed the failure of the conventional models to predict the analytical findings.

Table 3 shows the classical models used by different researchers to compare experimental findings in the present investigation. The underestimation of the experimental findings by the theoretical models is most probably due to the consideration of the NP's concentration, the TC of the host BFs, and the NPs only. However, as reported and investigated in the current study, the TC of the NFs is not limited to the subject parameters only. Still, it also depends upon the shape and size of the NPs used and the extent of dispersion and stability of the NPs in the host BFs.

5.3. Viscosity of ZnO/EG NFs

VC of ZnO/EG-based NFs varies inversely with the temperature and directly with the mass concentration of NPs, as presented in Fig. 6(a). For example, at 40 °C temperature, the rise in VC of NFs compared to EG was 5.42–15.22 % for 0.012–0.048 wt %. The depression in the VC of the NFs with the temperature rise is possibly due to the weakening of the interfacial layer resistance and, hence, van der Waals forces between the individual NPs. On the other hand, the rise in the VC with the increased concentration of NPs shows the increased resistance and shear forces among the coinciding NFs layers [58]. The maximum rise in the VC of the NFs was seen at the higher concentrations of the NPs and low temperatures. However, this rise was not significant at higher concentrations and temperatures, strengthening the consideration of studied NFs for high-temperature heat transfer systems. Similar findings have been observed in a study [48] with ZrO_2/EG-based NFs, with a volume concentration of 0.2–1.0 % and a temperature range of 20–60 °C. The VC of the ZrO_2/EG-based NFs augmented with the rise in the NPs loading, while it decreased with the system's operating temperature. The experimental results of the present study were compared with the aforementioned study at 60 °C. In the present case, the VC enhancement was 5.79–18.73 % for the NPs mass concentration of 0.012–0.048 %, while for ZrO_2/EG-based NFs, this enhancement was 7.66–39.23 % in the volume concentration of 0.2–1.0 %. The lower VC reported in the case of ZrO_2/EG-based NFs is observed compared to ZnO/EG-based NFs. The deviation of the current research results from the aforementioned study is possibly due to the different nature and physical properties of the NPs. This deviation in VC also shows that the VC is not only dependent on the operating temperature of the system but also on the nature of the NPs, the concentration of the NPs in the host BFs and the size and shape of the NPs. The current research findings were also compared and contrasted with a study [45] conducted by the authors using ZnO NPs in the DIW under similar concentrations of the NPs and operating temperatures, as presented in Fig. 6(b). It can be seen in Fig. 6(b) that in the case of DIW and EG base host BFs, the VC of NFs followed a similar trend with the NPs loading and the operating temperature. The comparison showed a decreasing trend in the VC of the NFs in both cases, while VC increased with the rise in the concentration of the NPs.

However, EG-based NFs showed relatively higher VC than DIW-based NFs under the same operating condition. This is possibly due to EG's relatively higher VC than DIW's. This also revealed that the NFs' VC is not only linked with the characteristics of the NPs but is also highly dependent upon the properties of the host BFs. Fig. 6(c) shows the percentage enhancement in the VC of the ZnO/EG-based NFs compared to the host BFs. It was recorded that the highest VC of the ZnO/EG-based NFs was at a temperature of 20 °C and a concentration of NPs of 0.048 wt %.

Fig. 6(d) compares the experimental findings for the ZnO/EG NFs with those estimated from the classical correlations. The investigation showed failure and underprediction of the experimental findings by the traditional classical models. Table 4 shows the classical models used by different researchers to compare experimental findings in the present investigation.

The underestimation of the experimental findings by the theoretical models is most probably due to the consideration of the NPs concentration only. However, as reported and investigated in the existing research study, the measured VC of the NFs is not limited to

Table 3
Classical models for predicting TC of NFs.

TC Models	Mathematical model	Remarks
Maxwell model [53]	$\frac{k_{eff}}{k_f} = \left[\frac{k_p + 2k_f + 2\Phi(k_f - k_p)}{k_p + 2k_f - \Phi(k_f - k_p)}\right]$	Based on the effective medium theory, uniformly dispersed and spherical-sized NPs.
Hamilton and Crosser [54]	$\frac{k_{eff}}{k_f} = \left[\frac{k_p + (n-1)k_f - (n-1)\Phi(k_f - k_p)}{k_p + (n-1)k_f + \Phi(k_f - k_p)}\right]$	Applicable for spherical and cylindrical particles. Developed by using the shape factor.
Timofeeva Model [55]	$\frac{k_{eff}}{k_f} = (1 + 3\varphi)$	Modelled considering the effective medium theory of NPs.
Wasp model [56]	$\frac{k_{eff}}{k_f} = \left[\frac{k_p + 2k_f - 2\Phi(k_f - k_p)}{k_p + 2k_f + \Phi(k_f - k_p)}\right]$	The shape factor is unity. Not valid for spherical particles.
Mintsa et al. [57]	$\frac{k_{eff}}{k_f} = (1 + 1.72\varphi)$	Concentration-dependent and non-temperature-dependent.

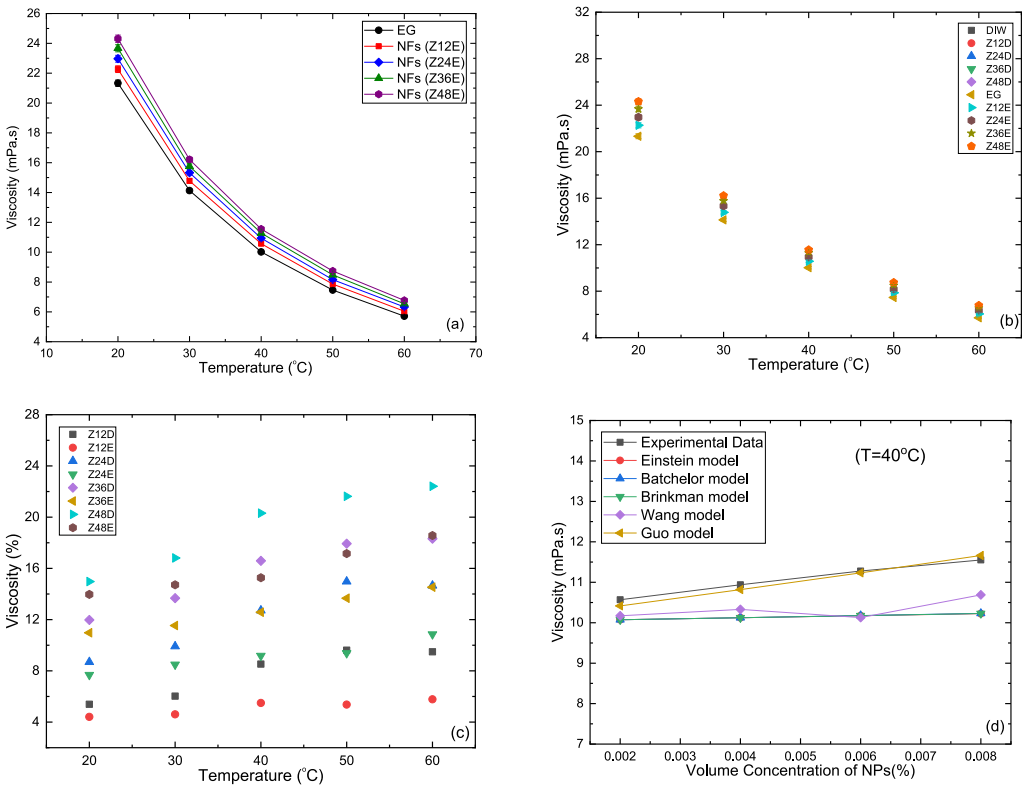

Fig. 6. ZnO/EG NFs VC (a) temperature vs NPs loading (b) comparison with classical models.

Table 4
Traditional classical correlations for predicting the VC of NFs.

Viscosity Model	Mathematical expression	Remarks
Einstein's model [59]	$\mu_{nf} = (1 + 2.5\varphi)\mu_f$	Applicable to the NPs of spherical shape only at volume fraction $\varphi < 0.02$.
Batchelor model [60]	$\mu_{nf} = (1 + 2.5\varphi + 6.5\varphi^2)\mu_f$	Modelled using Einstein's model and minding the Brownian motion of the NPs
Brinkman model [61]	$\mu_{nf} = (1 - \varphi^{2.5})\mu_f$	Applicable for continuous NPs medium for the NPs loading up to 4.0 %
Wang model [62]	$\mu_{eff} = \mu_f(1 + 7.3\varphi + 123\varphi^2)$	Formulated taking the standard room temperature as a reference for VC measurements.
Guo et al. [63]	$\mu_{eff} = \mu_f(1 + 2.5\varphi + 6.5\varphi^2)(1 + 350\varphi/d_p)$	Developed by considering the size and concentration of the NPs only in the host BFs.

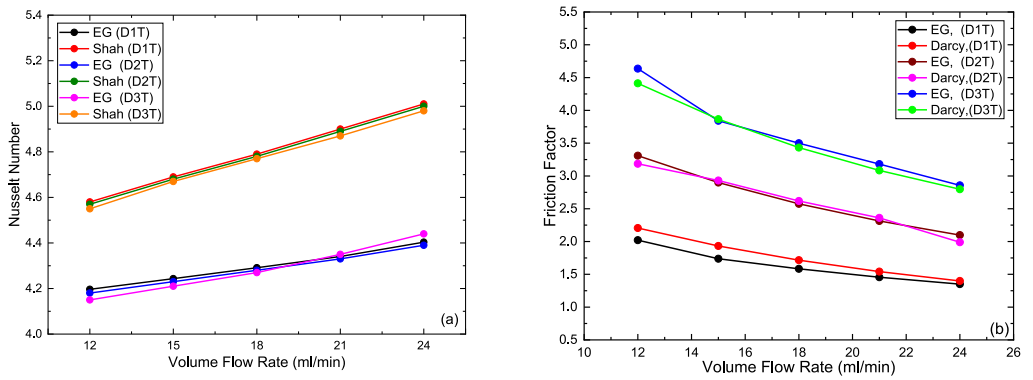

Fig. 7. Validation of experimental test setup for (a) Nusselt Number and (b) Friction Factor of NFs.

the subject parameters only. Instead, it also depends upon the operating temperature, shape, and size of the NPs used and the extent of dispersion and stability of the NPs in the host BFs.

5.4. Validation of test setup

In the current study, the research setup for investigating the thermal (HTC) performance and hydraulic features of the ZnO/EG-based NFs have been validated for the desired experimentation to check its accuracy using EG as a standard BFs. Therefore, the testing was made under the desired operating settings, and the results were evaluated to estimate the Nusselt number and frictional losses through the minichannel test tube.

The assessment of the results obtained for the subject parameters was made with the famous theoretical classical Shah correlation for the Nusselt number [64] and then with the Darcy Correlation for frictional losses [65], as presented in Fig. 7(a) and (b). The theoretical and analytical results have presented the highest deviation of ±5.86 % and ±2.80 %, respectively. These minor deviations are attributed to the possible minor variations in the controlled conditions, which are not considered in the theoretical models. However, the deviations are slight and can be considered in an acceptable range. Many researchers in the existing literature use the

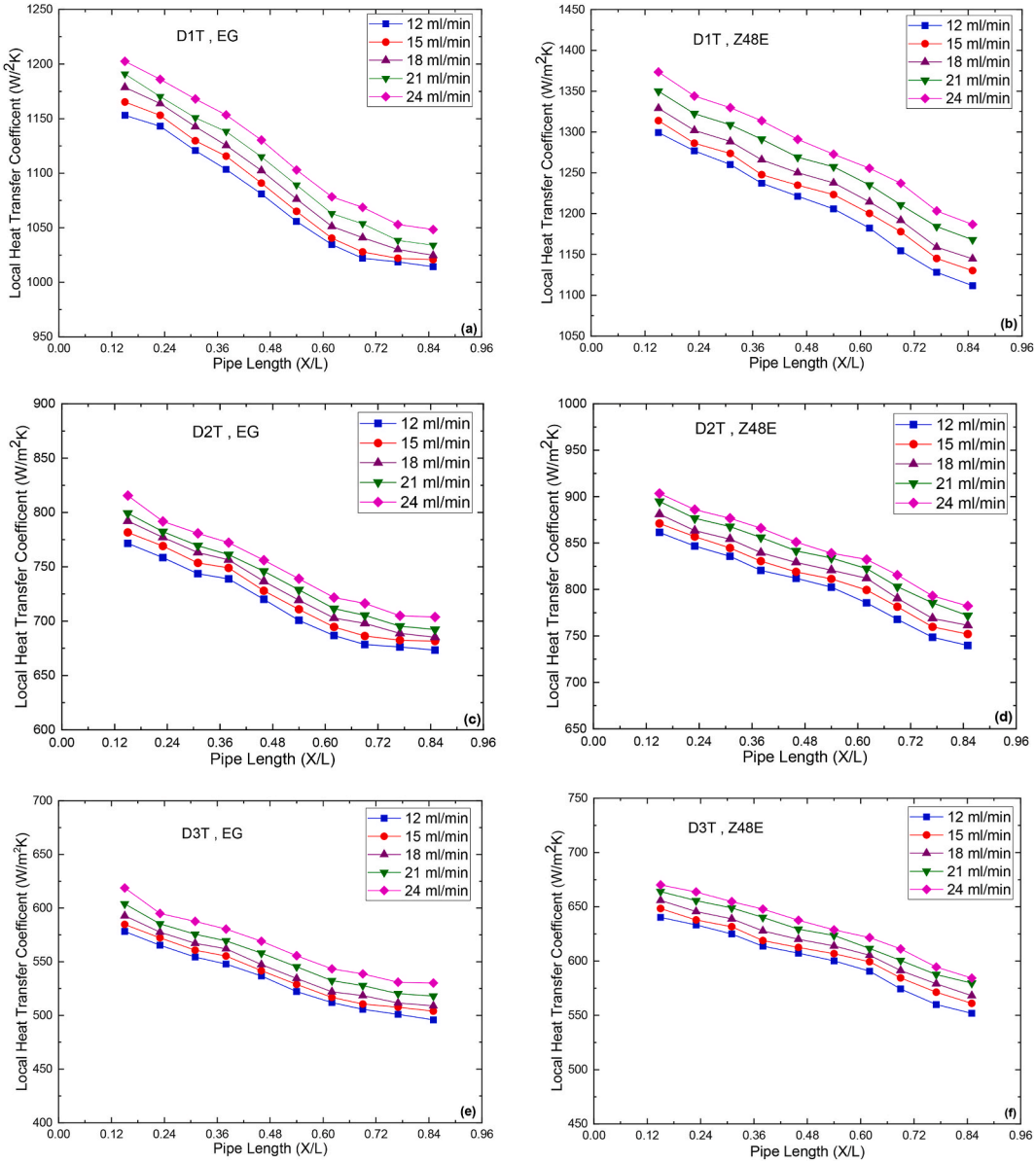

Fig. 8. Variations in local HTC of pure EG and NFs under varying tube diameters (a) EG, D1T,(b) Z48E, D1T (c) EG, D2T (d) Z48E, D2T (e) EG, D3T (f) Z48E, D3T.

subject correlations to validate compact channel-based experimental testing setups subjected to the constant heat flux in the laminar flow regime using NFs.

The findings confirmed the reasonable accuracy of the test rig for investigating the thermal (HTC) and hydraulic performance of ZnO/EG-based NFs within the designed operating conditions. Further, it confirms the repeatability and reproducibility of the experimental results within the examined uncertainties for the performance characteristics of the ZnO/EG-based NFs under the subject operating conditions.

5.5. Local heat transfer coefficient of ZnO/EG NFs

Fig. 8(a–f) presents the relationship between the local HTC and the non-dimensional pipe length of the mini tube test sections. For HTC, experiments were performed for NFs containing different concentrations of ZnO NPs ranging from 0.012 to 0.048 wt % and the mass flow rates ranging from 12.0 to 24.0 ml/min. The research findings revealed that local HTC is high at the channel's entry and progressively decreases with an increase in the direction of the test section length. At the entry level, the boundary layer of fluid is not fully developed, and HTC is high. However, approaching the developing region, the HTC decreases and attributes to attain a constant value for a fully developed flow. This behavior is due to the uniform temperature gradient between the flowing fluid within the test section and the temperature of the heated wall of the minichannel test sections. Similar findings were observed when the diameter of the test section was increased. The maximum enhancement recorded in local HTC against 0.048 wt % of NPs and 1.0 mm diameter (D1T) of the test section at 24.0 ml/min was 14.80 % compared with EG. The corresponding enhancement for the 1.5 mm (D2T) and 2.0 mm (D3T) diameter test sections was 10.76 % and 8.30 %, respectively.

The findings showed an enhancement in the local HTC with the rise in the concentration of the NPs, which is attributed to the thermal performance enhancement at the cost of an increase in the TC of the NFs. The HTC augmentation with the rise in flow rate at the cost of Reynolds number enrichment is also a prime factor. It also includes the increase in convective mass transfer role in triggering the thermal performance of NFs within the minichannel test section.

The other factors responsible for the enrichment of the thermal characteristics of the NFs include but are not limited to the enhancement in the TC of the NFs with the rise and mass concentration of NPs and the rise in the NFs flow rate within the minichannels.

The research findings also confirmed that the minichannel test sections with smaller diameters have great potential for high heat flux removal applications if the hydraulic characteristics of the NFs are not compromised much. Optimization between the NF's thermal characteristics and hydraulic performance within minichannels will lead to this novel concept for commercial applications.

Fig. 9(a) and (b) show a comparative analysis of experimental findings for HTC plotted against predicted values by Shah correlation [66] for pure EG and ZnO/EG-based NFs, respectively. The experimental findings were within 15 % of the projected values from the Shah correlation. The comparison shows that the experimental results for evaluating the thermal (HTC) performance of the ZnO/EG-based NFs in compact channel thermal systems in the developing and fully developed flow can be estimated with reasonable accuracy using the traditional classical correlations. The prediction of the experimental data through the classical mathematical models also reflects the fact of predicting the HTC of the NFs for other mass concentrations of NPs and the operating conditions to optimize the different parameters for higher HTC with a minimum compromise over the thermal and hydraulic characteristics of the NFs within the compact channels.

5.6. Average heat transfer coefficient of ZnO/EG NFs

Fig. 10(a–c) presents the average HTC of the ZnO/EG-based NFs in the minichannel test sections of different diameters under varying flow rates and mass loading of NPs. The average HTC was directly proportional with the NFs flow rate and the NPs loading. At the same time, an inverse relationship exists with the diameters of the test sections. The maximum enhancement recorded in the average HTC against 0.048 wt % of NPs and 1.0 mm diameter (D1T) of the test section at 24.0 ml/min was 13.48 % compared with EG.

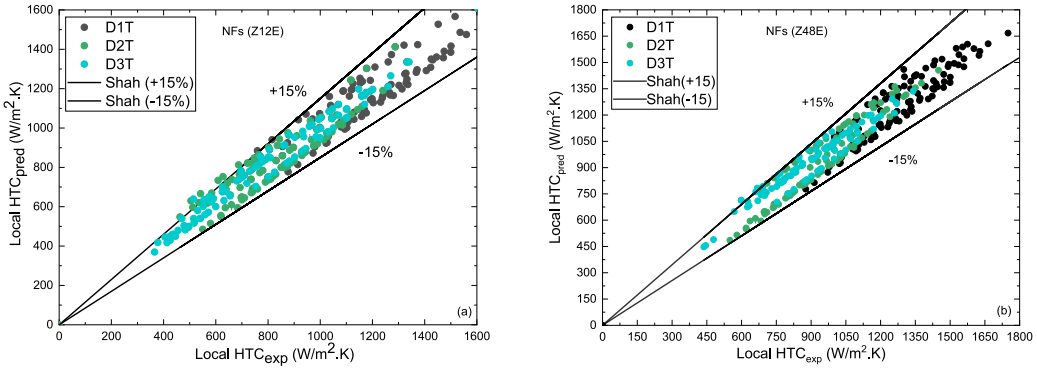

Fig. 9. Comparison of local HTC and results predicted from Shah correlation (a) Z12E (b) Z48E.

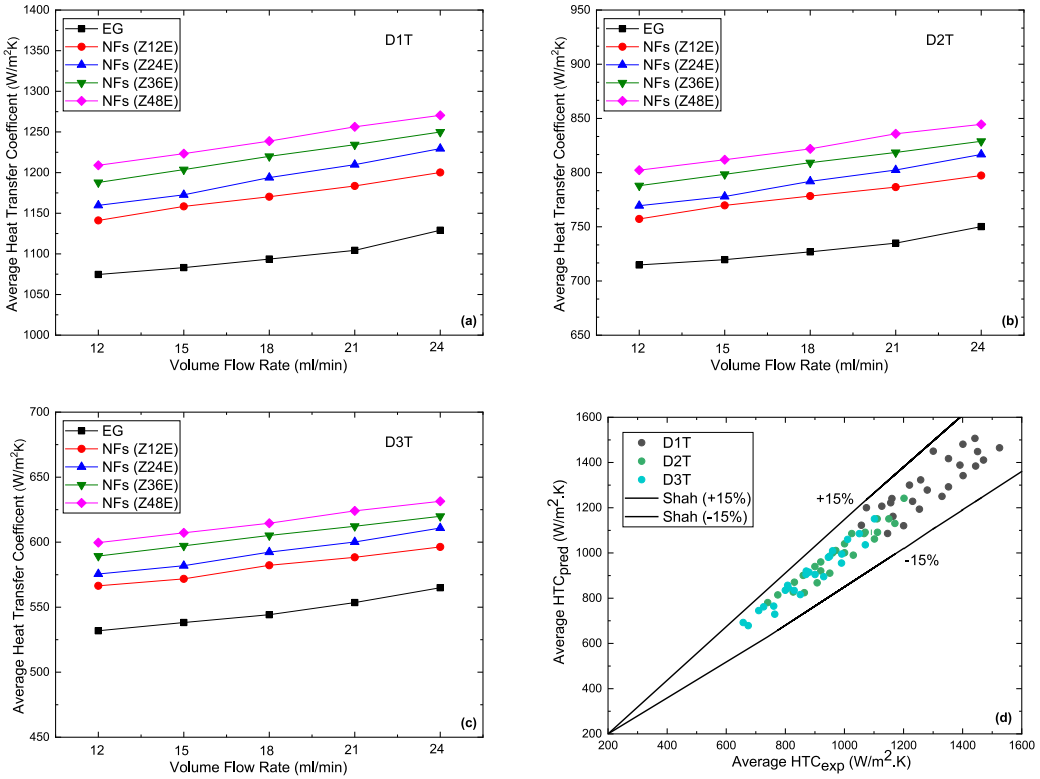

Fig. 10. Average HTC of ZnO-EG at (Z12E, Z24E, Z36E, Z48E) with volume flow rate (a) D1T (b) D2T (c) D3T (d) Comparison of average HTC with Shah correlation.

The corresponding enhancement for the 1.5 mm (D2T) and 2.0 mm (D3T) diameter mini tubes was 12.56 % and 11.75 %, respectively. The increased flow rate enhances the governing parameters affecting the HTC, while the NPs loading improves the thermal conduction within the host BFs. These factors ultimately boost the overall thermal performance of the NFs within the heat-exchanging system. The decrement in the inlet diameter impacts the velocity of the NFs and, hence, the Reynolds number, leading to an increase in heat transfer rate. The research findings were compared with the existing studies in the literature. A study by Sundar and Shaik [67] investigated the heat transfer performance of nanodiamond-based NFs in EG in a volume concentration of 0.2–1.0 %. Under constant heat flux and laminar flow conditions, as adopted in the present study, the study confirmed an enhancement in the HTC of NFs with the rise in Reynolds number and the mass concentration of NPs in the host BFs. They observed a maximum enhancement of 45.01 % in the HTC compared to the BFs. The comparison also shows that the HTC is also dependent upon the morphological characteristics and thermophysical properties of the NPs and NFs, respectively, and these are supposed to be a great influential parameter in heat transfer performance evaluation. Fig. 10(d) compares the experimental results and those predicted with the classical Shah Correlation [66] for ZnO/EG NFs. The findings showed that the deviation between the theoretical and analytical findings was within ±15 %. Adding NPs enhanced the average HTC due to the improved TC of the NFs and increased Brownian motion of NPs within the host BFs.

It also shows that smaller diameters are recommended for higher HTC if the other conditions are optimized. Similar reasons observed for local HTC also contribute to the enrichment of the average HTC. The average HTC presents the thermal performance of the bulk fluid corresponding to the bulk fluid temperature and the bulk mass transfer of the fluid during flow within the compact channels. In average HTC, the effects of the fluid flow behavior in the developing and fully developed region are not separately dealt with and is an uncomplicated representation of the fluid thermal performance within the flow channel without estimating the point-to-point temperatures across the surface subjected to the constant heat flux boundary conditions.

5.7. Average Nusselt number of ZnO/EG NFs

The average Nusselts number variation with volume flow rate for EG and ZnO/EG-based NFs is illustrated in Fig. 11(a–c). It is evident that the average Nusselt number increases with volume flow rate and NPs loadings but decreases with increasing test section diameters.

The maximum enhancement noted in the average Nusselts number for ZnO/EG-based NFs compared to BFs was 9.74 % against 0.048 wt % of NPs and 1.0 mm diameter (D1T) of the test section at 24.0 ml/min. The corresponding enhancement for the 1.5 mm (D2T) and 2.0 mm (D3T) diameter mini tubes was 8.85 % and 7.74 %, respectively. The research findings were compared with the

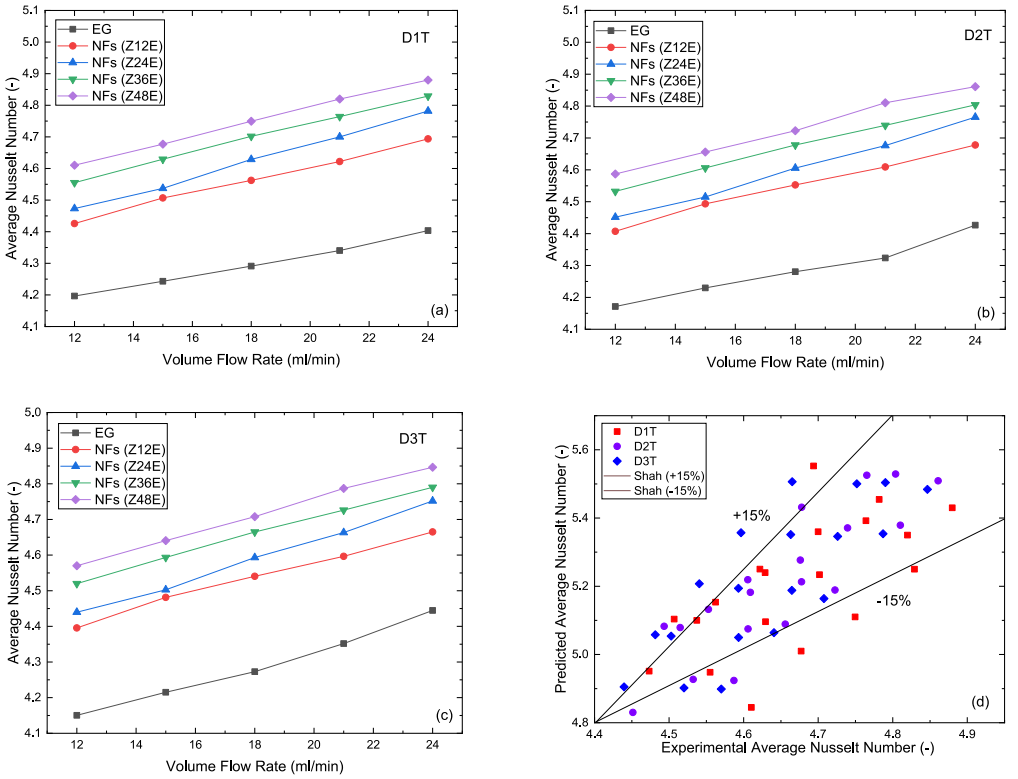

Fig. 11. Average Nusselt number of ZnO-EG at (Z12E, Z24E, Z36E, Z48E) with volume flow rate (a) D1T (b) D2T (c) D3T (d) Comparison of average Nusselt number with Shah correlation.

existing studies in the literature conducted by Sundar and Ramana [68]. The study confirmed an enhancement in the average Nusselts number with the rise in Reynolds number and NPs loading. They observed a maximum enhancement of 72.33 % in the Nusselt number at a 1.0 vol % compared to the BFs. The comparison also showed that the Nusselt number depends on the morphological characteristics and thermophysical properties of the NPs and NFs, respectively. Fig. 11(d) compares the experimental results and those predicted with the classical Shah Correlation [66] for ZnO/EG NFs. The findings showed that the deviation between most of the theoretical and analytical findings was within ±15 %.

5.8. *Pressure drop of ZnO/EG NFs*

Fig. 12(a–c) shows the hydraulic characteristics of the NFs under varying flow rate conditions, test section diameters, and the loading of the NPs. As usual, the pressure gradient intensified with the NPs loading and the volume flow rate of NFs. In contrast, an inverse proportion exists between the pressure drop and the area of the minichannel cross-section. The maximum pressure gradient observed for the test section of diameter 1.0 mm (D1T) was 32.16 % at 0.048 wt% mass concentration of NPs for 24.0 ml/min flow rate of the NFs.

The test sections' corresponding pressure drops for 1.5 mm (D2T) and 2.0 mm (D3T) diameters minichannel test tubes were recorded as 22.31 % and 13.88 %, respectively, compared to EG. The higher NPs concentration is attributed to more viscous forces at higher flow rates and contributes towards the more pressure gradient. By reducing the cross-sectional area of the test section, the per unit area exerted force by the flowing fluid enhances and increases the overall pressure gradient. The experimental findings in the laminar flow regime were also compared and contrasted with those predicted from the well-known classical Darcy correlation [69], as shown in Fig. 12(d).

The findings showed that the experimental results agreed with the predicted values within the ±10.0 % deviation range. This shows the validation of the prediction of the experimental results by the Darcy correlation [69] n in the existing literature, where different researchers have used it for the pressure drop modeling while dealing with a diverse range of NPs in various conventional and non-conventional channels for evaluating their hydraulic characteristics for heat transfer applications.

The hydraulic performance of the NFs within the minichannel heat exchangers of varying diameters showed that the larger inlet dimeters of the minichannels are best suited for the low-pressure drops across the test section, however, with a compromise over the HTC. Hence, optimizing the HTC and the hydraulic characteristics of the NFs should be critically considered while operating with the minichannel heat exchanging systems for thermal applications.

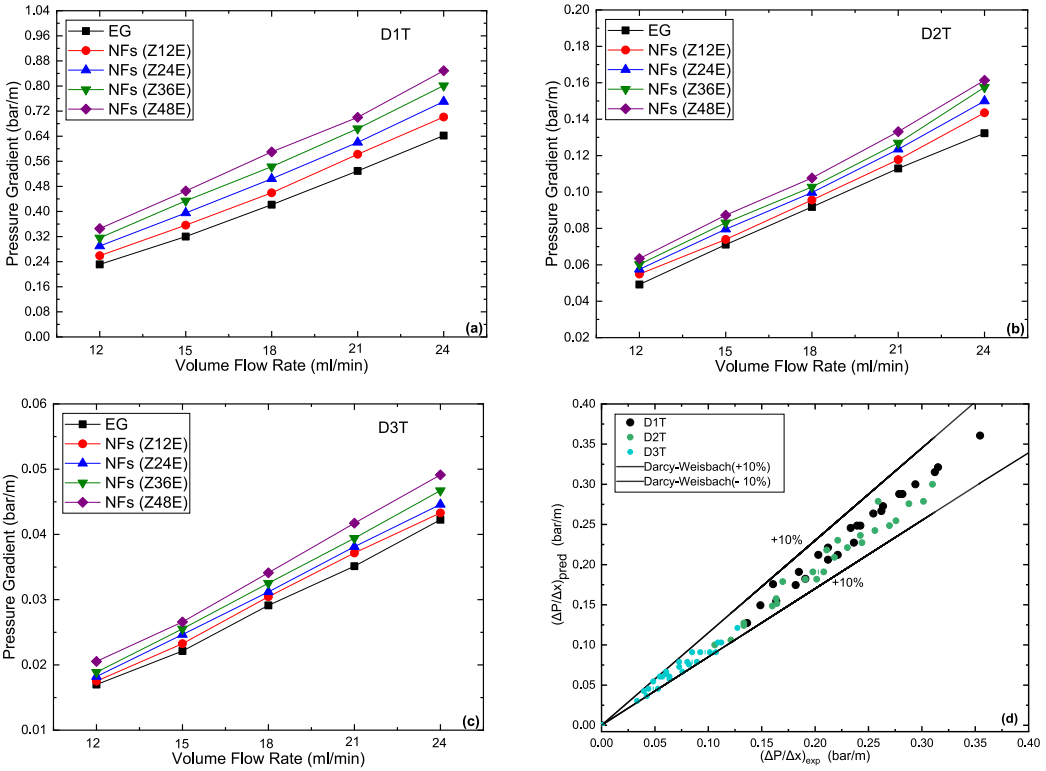

Fig. 12. Pressure gradient of ZnO-EG at (0.012, 0.024, 0.036, and 0.048 wt %) with volume flow rate (a) D1T (b) D2T (c) D3T (d) Comparison of pressure gradient from Darcy correlation.

5.9. Friction factor of ZnO/EG NFs

The friction factor (*f*) of the ZnO/EG-based NFs depends on the NP's loading within the host BFs and the flow rate of NFs. Therefore, the relation between the subject parameters and the friction factor (*f*) is well projected in Fig. 13(a–c). The friction factor increased with the NPs loading, while an opposite effect was observed with the NFs flow enrichment. It also possessed a direct proportion with the diameters of the test sections. The impact of the friction factor is more significant at lower fluid flow rates due to lower values of the Reynolds number, most probably due to the dominance of the viscous forces over the inertia force, leading to more frictional losses. The friction factor (*f*) of the formulated NFs, on the other hand, is also the function of the relative roughness of the minichannel flow systems. In the present case, for 0.048 wt % of NPs, the maximum friction factor at a 12.0 ml/min volume flow rate of NFs was 34.58 % in the test section of 1.0 mm diameter (D1T). The corresponding values for 1.5 mm (D2T) and 2.0 mm (D3T) diameter minichannel test tubes were 20.77 % and 15.96 %, respectively, compared to EG. The increased cross-sectional area of the flow channel depresses the velocity of the NFs, dominating inertia forces over viscous forces, and hence the frictional losses decrease. When the flow rate is very low, the role of the relative roughness of the system is negligible compared to the other dominating factors. Therefore, it does not influence the flow behaviour of the NFs within the compact channels.

The results of the current study were compared to a study by Sundar and Ramana [67], investigating the friction factor of Nano-diamond-based NFs in EG in a volume concentration of 0.2–1.0 %. Experiments were performed by applying constant heat flux under laminar flow conditions. Their observations showed that friction factor increased with NPs concentration but decreased with volume flow rate. The trend observed in the present research work matches with the aforementioned research findings. The maximum enhancement of 27.9 % in the friction factor for 1.0 wt % of NPs was observed compared to the BFs in their investigation. The friction factor in the present study was higher than the aforementioned findings, most probably due to the different nature, size, and shape of NPs, flow conditions, and other operating parameters.

Fig. 13(d) compares experimental findings with those predicted by the well-known classical Darcy correlation [69] in the laminar flow regime. It shows that the experimental findings agreed with the predicted values for fiction factor in the tubes of different diameters for all volume flow NPs loadings within the ±10.0 % deviation range. The agreement between the experimental and theoretical results shows that the data reflects the reasonable accuracy of the experimental setup. Many researchers have also used the Darcy correlation [69] in the laminar flow regime in the existing literature to predict the friction factor. It is well-mapped with the findings in the current study.

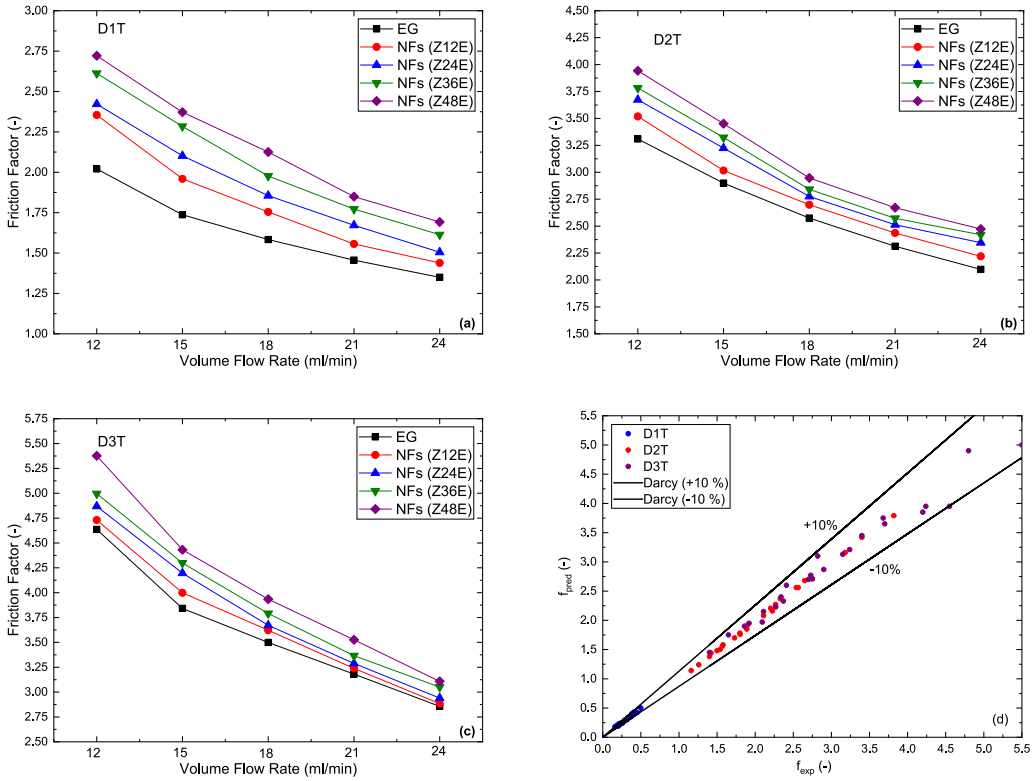

Fig. 13. Friction factor of ZnO-EG at (0.012, 0.024, 0.036, and 0.048 wt %) with volume flow rate (a) D1T (b) D2T (c) D3T (d) Comparison of friction factor with Darcy correlation.

6. Conclusion and future recommendations

The thermal and hydraulic performance of ZnO/EG-based NFs were investigated in minichannel heat exchangers of different inner diameters under constant heat flux and laminar flow conditions. The following conclusions have been drawn from the experimental findings for the NFs investigated in this study.

1. The TC and VC increased with the NP's loading. In addition, TC increased with the increase in the NFs temperature, while the VC of the NFs showed an inverse behavior under the same operating conditions. Under steady-state operating conditions, the enhancement in the subject properties of the NFs was 13.80 % and 15.22 %, respectively. The enhancement in TC of NFs with increased NPs loading and operating temperature is attributed to the thermal percolation, NPs to BFs interaction, higher TC of NPs, and increased Brownian motion of NPs in the host BFs. On the other hand, NPs to BFs interaction increases with the rise in NP concentration, leading to increased VC of NFs. However, the decrease in the VC with the temperature rise is due to reduced interparticle van der Waals and electrostatic forces.
2. Both the local HTC and the average HTC possessed an increasing trend with mass loading of the NPs and the NFs volume flow rate. However, HTC showed an inverse trend with the variation in the inlet diameter of the minichannel test section due to possible variations in the Reynold number of the NFs system. Under the standard operating conditions, the local and average HTC enhancement was 14.80 % and 13.48%, respectively. The enhancement in HTC with the NP's loading is attributed to the enhanced TC of the BFs and increased Brownian motion of NPs. The convective HTC also increases with the increase in volume flow rate, leading to an increase in overall local and average HTC. However, an increase in the cross-sectional area of the test section inlet directly impacts the velocity of the NFs and, hence, the HTC.
3. Both the friction factor and the pressure gradient across the test section possessed an increasing trend with the loading of the NPs. However, the friction factor (f)was directly proportional to the compact channels' cross-sectional area, while the pressure gradient showed an inverse behavior. An opposite behavior was observed in the case of comparison over the volume flow rate. For the standard operating conditions, the maximum friction factor (f) and the pressure drop for all three test sections of the different diameters were recorded as 34.58 % and 32.16 %, respectively. The enhancement in the friction factors and the pressure gradient due to NPs loading attributes to the increased VC, higher velocity gradients, and additional shear stress effects between the NPs and the host BFs. The effect of minichannels cross-sectional area on the friction factor and the pressure gradient is also attributed to the aforementioned parameters.

4. The experimental results for local and average HTC were within ±15.0 % of those predicted from the well-known Shah correlation. However, the experimental findings were within the ±10.0 % range of the predicted results from the notable Darcy correlation for the friction factor and the pressure gradient. This shows that existing correlations for the subject parameters can reasonably predict the experimental findings. However, the slight deviations observed are due to different morphological characteristics of the NPs and the design operating conditions that are inconsistent with those considered in the classical correlations.

The research findings showed the potential of the ZnO/EG-based NFs for thermal applications by integrating mini and microchannels of different diameters. The lower diameter test sections could enhance the HTC to a great extent but compromise the hydraulic performance of the NFs and vice versa. However, there is still a potential to optimize the cross-sectional area of the mini and microchannel heat exchangers with a minimum compromise over the aforementioned characteristics of the NFs. This could be the potential research area for thermal engineers working in microfluidics and nanofluidics for their potential applications in the next generation of high heat flux thermal systems.

CRediT authorship contribution statement

Muhammad Ahsan: Writing – original draft, Investigation, Data curation. **Adnan Qamar:** Writing – original draft, Formal analysis, Conceptualization. **Rabia Shaukat:** Writing – review & editing, Investigation. **Habib-ur-Rehman Siddiqi:** Writing – review & editing, Formal analysis. **Zahid Anwar:** Writing – review & editing. **Muhammad Farooq:** Writing – review & editing. **Muhammad Amjad:** Writing – review & editing, Validation. **Shahid Imran:** Writing – review & editing, Project administration. **Mansoor Ahmed:** Writing – review & editing. **M.A. Mujtaba:** Writing – review & editing, Software. **H. Fayaz:** Writing – review & editing, Funding acquisition. **Basma Souayeh:** Writing – review & editing, Funding acquisition.

Declaration of competing interest

The authors declare that they have no known competing financial interests or personal relationships that could have appeared to influence the work reported in this paper.

Acknowledgment

The authors thank the University of Engineering and Technology (UET), Lahore, Pakistan, for their invaluable support and resources, especially through Research Grants No. ORIC/105-ASRB/3084, ORIC/101-ASRB/4452, and ORIC/101-ASRB/4453 significantly advanced our research endeavors. Furthermore, the authors express profound appreciation to the Pakistan Science Foundation (PSF) for their generous funding and pivotal role in facilitating this research project, particularly under Research Grant No. PSF/CRP/8th/P-UET/Consrm-(06).

References

[1] S.M. Sohel Murshed, C.A. Nieto de Castro, A critical review of traditional and emerging techniques and fluids for electronics cooling, Renew. Sustain. Energy Rev. 78 (2017) 821–833, https://doi.org/10.1016/j.rser.2017.04.112.
[2] S.U.S. Choi, J.A. Eastman, Enhancing thermal conductivity of fluids with nanoparticles, ASME Int. Mech. Eng. Congr. Expo. 66 (1995) 99–105, https://doi.org/10.1115/1.1532008.
[3] T.A. Moreira, D.C. Moreira, G. Ribatski, Nanofluids for heat transfer applications: a review, J. Brazilian Soc. Mech. Sci. Eng. 40 (6) (2018), https://doi.org/10.1007/s40430-018-1225-2.
[4] R.B. Ganvir, P.V. Walke, V.M. Kriplani, Heat transfer characteristics in nanofluid-A review, Renew. Sustain. Energy Rev. 75 (2017) 451–460, https://doi.org/10.1016/j.rser.2016.11.010.
[5] M. Gupta, V. Singh, R. Kumar, Z. Said, A review on thermophysical properties of nanofluids and heat transfer applications, Renew. Sustain. Energy Rev. 74 (2017) 638–670, https://doi.org/10.1016/j.rser.2017.02.073.
[6] K.S. Suganthi, K.S. Rajan, Metal oxide nanofluids: review of formulation, thermophysical properties, mechanisms, and heat transfer performance, Renew. Sustain. Energy Rev. 76 (2017) 226–255.
[7] G. Liang, I. Mudawar, Review of single-phase and two-phase nanofluid heat transfer in macro-channels and micro-channels, Int. J. Heat Mass Tran. 136 (2019) 324–354, https://doi.org/10.1016/j.ijheatmasstransfer.2019.02.086.
[8] A.M. Hussein, K. Kadirgama, M.M. Noor, Nanoparticles suspended in ethylene glycol thermal properties and applications: an overview, Renew. Sustain. Energy Rev. 69 (November) (2016) 1, https://doi.org/10.1016/j.rser.2016.12.047.
[9] A. Kaggwa, J.K. Carson, M. Atkins, M. Walmsley, The effect of surfactants on viscosity and stability of activated carbon, alumina and copper oxide nanofluids, Mater. Today Proc. 18 (2019) 510–519, https://doi.org/10.1016/j.matpr.2019.06.240.
[10] C. Jumpholkul, O. Mahian, A. Kasaeian, A.S. Dalkilic, S. Wongwises, An experimental study to determine the maximum efficiency index in turbulent flow of SiO2/water nanofluids, Int. J. Heat Mass Tran. 112 (2017) 1113–1121, https://doi.org/10.1016/j.ijheatmasstransfer.2017.05.007.
[11] H.L. Yurong He, Yi Jin, Haisheng Chen, Yulong Ding, Daqiang Cang, Heat transfer and flow behaviour of aqueous suspensions of TiO2 nanoparticles (nanofluids) flowing upward through a vertical pipe, Int. J. Heat Mass Tran. 50 (2007) 2272–2281.
[12] M.J. Pastoriza-Gallego, L. Lugo, J.L. Legido, M.M. Piñeiro, Thermal conductivity and viscosity measurements of ethylene glycol-based Al2O3 nanofluids, Nanoscale Res. Lett. 6 (1) (2011) 1–11, https://doi.org/10.1186/1556-276X-6-221.
[13] P.K. Kanti, M.P. Maiya, Rheology and thermal conductivity of graphene oxide and coal fly ash hybrid nanofluids for various particle mixture ratios for heat transfer applications: experimental study, Int. Commun. Heat Mass Tran. 138 (September) (2022) 106408, https://doi.org/10.1016/j.icheatmasstransfer.2022.106408.
[14] N.R. Karthikeyan, J. Philip, B. Raj, Effect of clustering on the thermal conductivity of nanofluids, Mater. Chem. Phys. 109 (2008) 50–55, https://doi.org/10.1016/j.matchemphys.2007.10.029.
[15] W. Guo, G. Li, Y. Zheng, C. Dong, Measurement of the thermal conductivity of SiO2 nanofluids with an optimized transient hot wire method, Thermochim. Acta 661 (2018) 84–97, https://doi.org/10.1016/j.tca.2018.01.008.

[16] S.S. Sonawane, R.S. Khedkar, K.L. Wasewar, Effect of sonication time on enhancement of effective thermal conductivity of nano TiO2-water, ethylene glycol, and paraffin oil nanofluids and models comparisons, J. Exp. Nanosci. 10 (2015) 310–322, https://doi.org/10.1080/17458080.2013.832421.
[17] J. Jeong, C. Li, Y. Kwon, J. Lee, S. Hyung, R. Yun, Particle shape effect on the viscosity and thermal conductivity of ZnO nanofluids, Int. J. Refrig. 36 (8) (2013) 2233–2241, https://doi.org/10.1016/j.ijrefrig.2013.07.024.
[18] H. Li, L. Wang, Y. He, Y. Hu, J. Zhu, B. Jiang, Experimental investigation of thermal conductivity and viscosity of ethylene glycol based ZnO nanofluids, Appl. Therm. Eng. 88 (2014) 363–368, https://doi.org/10.1016/j.applthermaleng.2014.10.071.
[19] M.J.P. Gallego, L. Lugo, D. Cabaleiro, J.L. Legido, M.M. Piñeiro, Thermophysical profile of ethylene glycol-based ZnO nanofluids, J. Chem. Thermodyn. 73 (2014) 23–30, https://doi.org/10.1016/j.jct.2013.07.002.
[20] M. Kole, T.K. Dey, Effect of prolonged ultrasonication on the thermal conductivity of ZnO – ethylene glycol nanofluids, Thermochim. Acta 535 (2012) 58–65, https://doi.org/10.1016/j.tca.2012.02.016.
[21] M. Moosavi, E.K. Goharshadi, A. Youssefi, Fabrication, characterization, and measurement of some physicochemical properties of ZnO nanofluids, Int. J. Heat Fluid Flow 31 (4) (2010) 599–605, https://doi.org/10.1016/j.ijheatfluidflow.2010.01.011.
[22] W. Yu, H. Xie, L. Chen, Y. Li, Investigation of thermal conductivity and viscosity of ethylene glycol based ZnO nanofluid, Thermochim. Acta 491 (1–2) (2009) 92–96, https://doi.org/10.1016/j.tca.2009.03.007.
[23] K.S.R.K. Rohini Priya, K.S. Suganthi, Transport properties of ultra-low concentration CuO-water nanofluids containing non-spherical nanoparticles, Int. J. Heat Mass Tran. 55 (2012) 4734–4743.
[24] W. Duangthongsuk, S. Wongwises, Measurement of temperature-dependent thermal conductivity and viscosity of TiO2-water nanofluids, Exp. Therm. Fluid Sci. 33 (4) (2009) 706–714, https://doi.org/10.1016/j.expthermflusci.2009.01.005.
[25] A. Qamar, et al., Dispersion stability and rheological characteristics of water and ethylene glycol based ZnO nanofluids, Therm. Sci. 25 (3) (2021) 1989–2001, https://doi.org/10.2298/TSCI200110187Q.
[26] V. Vicki Wanatasanappan, P. Kumar Kanti, P. Sharma, N. Husna, M.Z. Abdullah, Viscosity and rheological behavior of Al2O3-Fe2O3/water-EG based hybrid nanofluid: a new correlation based on mixture ratio, J. Mol. Liq. 375 (2023) 121365, https://doi.org/10.1016/j.molliq.2023.121365.
[27] K.B. Anoop, T. Sundararajan, S.K. Das, Effect of particle size on the convective heat transfer in nanofluid in the developing region, Int. J. Heat Mass Tran. 52 (2009) 2189–2195, https://doi.org/10.1016/j.ijheatmasstransfer.2007.11.063.
[28] U. Rea, T. Mckrell, L. Hu, J. Buongiorno, Laminar convective heat transfer and viscous pressure loss of alumina-water and zirconia-water nanofluids, Int. J. Heat Mass Tran. 52 (2009) 2042–2048, https://doi.org/10.1016/j.ijheatmasstransfer.2008.10.025.
[29] K. Goudarzi, H. Jamali, Heat transfer enhancement of Al2O3-EG nanofluid in a car radiator with wire coil inserts, Appl. Therm. Eng. 118 (2017) 510–517, https://doi.org/10.1016/j.applthermaleng.2017.03.016.
[30] A. Abdollahi, H.A. Mohammed, S.M. Vanaki, A. Osia, M.R. Golbahar Haghighi, Fluid flow and heat transfer of nanofluids in microchannel heat sink with V-type inlet/outlet arrangement, Alex. Eng. J. 56 (2017) 161–170, https://doi.org/10.1016/j.aej.2016.09.019.
[31] M. Gupta, R. Kumar, N. Arora, S. Kumar, N. Dilbagi, Experimental investigation of the convective heat transfer characteristics of TiO2/distilled water nanofluids under constant heat flux boundary condition, J. Brazilian Soc. Mech. Sci. Eng. 37 (4) (2015) 1347–1356, https://doi.org/10.1007/s40430-014-0262-8.
[32] S.M.H. Hashemi, S.A. Fazeli, H. Zirakzadeh, M. Ashjaee, Study of heat transfer enhancement in a nanofluid-cooled miniature heat sink, Int. Commun. Heat Mass Tran. 39 (6) (2012) 877–884, https://doi.org/10.1016/j.icheatmasstransfer.2012.04.005.
[33] M.A.N. Hafiz Muhammad Ali, Hassan Ali, Liaquat Hassan, Hafiz Talha Bin Maqsood, Experimental investigation of convective heat transfer augmentation for car radiator using ZnO/water nanofluids, Energy 84 (2015) 317–324, https://doi.org/10.1016/j.energy.2015.02.103.
[34] A. Topuz, T. Engin, A. Alper Özalp, B. Erdoğan, S. Mert, A. Yeter, Experimental investigation of optimum thermal performance and pressure drop of water-based Al2O3, TiO2 and ZnO nanofluids flowing inside a circular microchannel, J. Therm. Anal. Calorim. 131 (2018) 2843–2863, https://doi.org/10.1007/s10973-017-6790-6.
[35] T. Wen, L. Lu, S. Zhang, H. Zhong, Experimental study and CFD modelling on the thermal and flow behavior of EG/water ZnO nanofluid in multiport mini channels, Appl. Therm. Eng. 182 (August 2020) (2021) 116089, https://doi.org/10.1016/j.applthermaleng.2020.116089.
[36] M.S. Alam, B. Nahar, M.A. Gafur, G. Seong, M.Z. Hossain, Forced convective heat transfer coefficient measurement of low concentration nanorods ZnO–ethylene glycol nanofluids in laminar flow, Nanomaterials 12 (9) (2022), https://doi.org/10.3390/nano12091568.
[37] Y.A.W. Ahmed, N. A Che Sidik, Metal oxide and ethylene glycol based well stable nanofluids for mass flow in closed conduit, J. Adv. Res. Micro Nano Eng. 1 (1) (2021) 1–15.
[38] P.K. Kanti, K.V. Sharma, A.A. Minea, V. Kesti, Experimental and computational determination of heat transfer, entropy generation and pressure drop under turbulent flow in a tube with fly ash-Cu hybrid nanofluid, Int. J. Therm. Sci. 167 (April) (2021) 107016, https://doi.org/10.1016/j.ijthermalsci.2021.107016.
[39] P.K. Kanti, K.V. Sharma, Z. Said, M. Gupta, Experimental investigation on thermo-hydraulic performance of water-based fly ash–Cu hybrid nanofluid flow in a pipe at various inlet fluid temperatures, Int. Commun. Heat Mass Tran. 124 (April) (2021) 105238, https://doi.org/10.1016/j.icheatmasstransfer.2021.105238.
[40] M. H B, P.K. Kanti, S.B. Prakash, S.N. Sridhara, Investigation of entropy generation and thermohydraulic characteristics of Al2O3–CuO hybrid nanofluid flow in a pipe at different inlet fluid temperatures, Int. J. Therm. Sci. 193 (July) (2023) 108541, https://doi.org/10.1016/j.ijthermalsci.2023.108541.
[41] A. Qamar, Z. Anwar, H. Ali, S. Imran, R. Shaukat, M. Mujtaba Abbas, Experimental investigation of dispersion stability and thermophysical properties of ZnO/DIW nanofluids for heat transfer applications, Alex. Eng. J. 61 (5) (2022) 4011–4026, https://doi.org/10.1016/j.aej.2021.09.028.
[42] A. Qamar, et al., Preparation and dispersion stability of aqueous metal oxide nanofluids for potential heat transfer applications: a review of experimental studies, J. Therm. Anal. Calorim. (2020) 0123456789, https://doi.org/10.1007/s10973-020-10372-z.
[43] W.T. Urmi, M.M. Rahman, K. Kadirgama, D. Ramasamy, M.A. Maleque, An overview on synthesis, stability, opportunities and challenges of nanofluids, Mater. Today Proc. 41 (2020) 30–37, https://doi.org/10.1016/j.matpr.2020.10.998.
[44] G. Paul, M. Chopkar, I. Manna, P.K. Das, Techniques for measuring the thermal conductivity of nanofluids: a review, Renew. Sustain. Energy Rev. 14 (2010) 1913–1924, https://doi.org/10.1016/j.rser.2010.03.017.
[45] H. Siddiqi, et al., Heat transfer and pressure drop characteristics of ZnO/DIW based nanofluids in small diameter compact channels : an experimental study, Case Stud. Therm. Eng. 39 (September) (2022) 102441, https://doi.org/10.1016/j.csite.2022.102441.
[46] J. Andraos, On the propagation of statistical errors for a function of several variables, J. Chem. Educ. 73 (2) (1996) 150–154.
[47] G.J. Lee, C.K. Kim, M.K. Lee, C.K. Rhee, S. Kim, C. Kim, Thermal conductivity enhancement of ZnO nanofluid using a one-step physical method, Thermochim. Acta 542 (2012) 24–27, https://doi.org/10.1016/j.tca.2012.01.010.
[48] L.S. Sundar, H.K. Mewada, Experimental study for thermophysical properties of ZrO/ethylene glycol nanofluid: developing an ANFIS modeling and proposing new correlations, J. Nanofluids 12 (5) (2023) 1440–1453, https://doi.org/10.1166/jon.2023.2018.
[49] K.E. Ramohlola, E.I. Iwuoha, M.J. Hato, K.D. Modibane, Instrumental techniques for characterization of molybdenum disulphide nanostructures, J. Anal. Methods Chem. 2020 (1) (2020), https://doi.org/10.1155/2020/8896698.
[50] P. Kumar Kanti, P. Sharma, K.V. Sharma, M.P. Maiya, The effect of pH on stability and thermal performance of graphene oxide and copper oxide hybrid nanofluids for heat transfer applications: application of novel machine learning technique, J. Energy Chem. 82 (2023) 359–374, https://doi.org/10.1016/j.jechem.2023.04.001.
[51] P.K. Kanti, P. Sharma, M.P. Maiya, K.V. Sharma, The stability and thermophysical properties of Al2O3-graphene oxide hybrid nanofluids for solar energy applications: application of robust autoregressive modern machine learning technique, Sol. Energy Mater. Sol. Cells 253 (July 2022) (2023) 112207, https://doi.org/10.1016/j.solmat.2023.112207.
[52] R.V. Pinto, F.A.S. Fiorelli, Review of the mechanisms responsible for heat transfer enhancement using nanofluids, Appl. Therm. Eng. 108 (2016) 720–739, https://doi.org/10.1016/j.applthermaleng.2016.07.147.
[53] J.C. Maxwell, A Treatise on Electricity and Magnetism, third ed., vol. 53, Clarendon Press, Oxford, UK, 1954, pp. 1–30, https://doi.org/10.1017/CBO9781107415324.004, 1891, A treatise Electr. Magn.

[54] R.L. Hamilton, O.K. Crosser, Thermal conductivity of heterogeneous two-component systems, Ind. Eng. Chem. Fundam. 1 (3) (1962) 187–191, https://doi.org/10.1021/i160003a005.
[55] E.V. Timofeeva, et al., Thermal conductivity and particle agglomeration in alumina nanofluids: experiment and theory, Phys. Rev. E - Stat. Non-linearr, Soft Matter Phys. 76 (6) (2007) 28–39, https://doi.org/10.1103/PhysRevE.76.061203.
[56] E.J. Wasp, J.P. Kenny, R.L. Gandhi, Solid-liquid Flow: Slurry Pipeline transportation.[Pumps, Valves, Mechanical Equipment, Economics], vol. 1, 1977 no. (United States).
[57] H.A. Mintsa, G. Roy, C.T. Nguyen, D. Doucet, New temperature dependent thermal conductivity data for water-based nanofluids, Int. J. Therm. Sci. 48 (2) (2009) 363–371, https://doi.org/10.1016/j.ijthermalsci.2008.03.009.
[58] M. Awais, A.A. Bhuiyan, S. Salehin, M.M. Ehsan, B. Khan, M.H. Rahman, Synthesis, heat transport mechanisms and thermophysical properties of nanofluids: a critical overview, Int. J. Thermofluids 10 (2021) 100086, https://doi.org/10.1016/j.ijft.2021.100086.
[59] A. Einstein, A new determination of molecular dimensions, Ann. Phys. 19 (1906) 289–306. . [Online]. Available: http://ci.nii.ac.jp/naid/10015778632/en/. (Accessed 14 March 2018).
[60] G.K. Batchelor, The effect of Brownian motion on the bulk stress in a suspension of spherical particles, J. Fluid Mech. 83 (1) (1977) 97–117, https://doi.org/10.1017/S0022112077001062.
[61] H.C. Brinkman, The viscosity of concentrated suspensions and solutions, J. Chem. Phys. 20 (4) (1952) 571–581, https://doi.org/10.1122/1.549141.
[62] X. Xu, S.U.S. Choi, X. Wang, Thermal conductivity of nanoparticle - fluid mixture, J. Thermophys. Heat Tran. 13 (4) (1999) 474–480.
[63] T. Wen, L. Lu, H. Zhong, B. Shen, Thermal properties measurement and performance evaluation of water/ZnO nanofluid in a mini channel with offset fins, Int. J. Heat Mass Tran. 162 (2020) 120361, https://doi.org/10.1016/j.ijheatmasstransfer.2020.120361.
[64] K.P. Venkitaraj, S. Suresh, T. Alwin Mathew, B.S. Bibin, J. Abraham, An experimental investigation on heat transfer enhancement in the laminar flow of water/TiO2 nanofluid through a tube heat exchanger fitted with modified butterfly inserts, Heat Mass Transf. und Stoffuebertragung 54 (3) (2018) 813–829, https://doi.org/10.1007/s00231-017-2174-5.
[65] M. Qasim, M. Sajid Kamran, M. Ammar, M. Ali Jamal, M. Yasar Javaid, Heat transfer enhancement of an automobile engine radiator using ZnO water base nanofluids, J. Therm. Sci. 29 (4) (2020) 1010–1024, https://doi.org/10.1007/s11630-020-1263-9.
[66] E.B. Haghighi, et al., Cooling performance of nanofluids in a small diameter tube, Exp. Therm. Fluid Sci. 49 (2013) 114–122, https://doi.org/10.1016/j.expthermflusci.2013.04.009.
[67] L.S. Sundar, F. Shaik, Laminar convective heat transfer, entropy generation, and exergy efficiency studies on ethylene glycol based nanofluid containing nanodiamond nanoparticles, Diam. Relat. Mater. 131 (November 2022) (2023) 109599, https://doi.org/10.1016/j.diamond.2022.109599.
[68] L.S. Sundar, E.V. Ramana, Influence of magnetic field location on the heat transfer and friction factor of CoFe2O4-BaTiO3/EG hybrid nanofluids in laminar flow: an experimental study, J. Magn. Magn Mater. 579 (April) (2023) 170837, https://doi.org/10.1016/j.jmmm.2023.170837.
[69] H. Almohammadi, S.N. Vatan, E. Esmaeilzadeh, A. Motezaker, A. Nokhosteen, Experimental investigation of convective heat transfer and pressure drop of Al2O3/water nanofluid in laminar flow regime inside a circular tube, World Acad. Sci. Eng. Technol. 68 (8) (2012) 2208–2213.